MATHEMATICAL MODELLING OF PARTICLE SEGREGATION DURING CENTRIFUGAL CASTING OF METAL-MATRIX COMPOSITES

A thesis submitted in partial fulfillment of the Requirements for the Degree of

MASTER OF TECHNOLOGY

By

Emila Panda

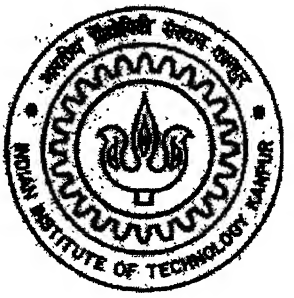

to the

DEPARTMENT OF MATERIALS AND METALLURGICAL ENGINEERING
INDIAN INSTITUTE OF TECHNOLOGY, KANPUR-208016

CERTIFICATE

This is to certify that the present work "*Mathematical Modelling of Particle Segregation during Centrifugal Casting of Metal-Matrix Composites*", by Emila Panda has been carried out under our supervision and that this has not been submitted elsewhere for a degree.

(Dr. S.P. Mehrotra)
Director
National Metallurgical Laboratory (NML),
Jamshedpur

(Dr.Dipak Mazumdar)
Professor
Dept. of Materials and Metallurgical Engg.
I. I.T., Kanpur

Dated: August 2003

ACKNOWLEDGEMENTS

I would like to take this opportunity to express my deep sense of gratitude to my supervisors Dr.S.P.Mehrotra and Dr.Dipak Mazumdar for their expert guidance and continuous encouragement through out the course of this work. I am sincerely thankful for their intellectual support and creative criticism which led me to generate my own ideas and made my work interesting and enjoyable.

I express my special thanks to my friends Bijayani, Mamta, Neeru, Anjana, Shiba, Ranjan bhai, Satish, Sriram, Abani, Madan, Jayant and many others for their suggestions during my course of study at IIT, Kanpur.

I have no words to express my thanks to my parents and my family members who have been constant source of inspiration to me. I wish to thank all my friends and well wishers who made my stay at IIT, Kanpur, memorable and pleasant.

CONTENTS

ABSTRACT

The metal matrix composites, have proved to be an important class of materials, with the potential to replace a number of conventional materials being used in automotive, aerospace, defense, and leisure industries, where the demand for light weight and higher strength components is increasing. During centrifugal casting of Aluminium melts containing suspended ceramic particles, segregation of the particles occurs either towards the outer or towards the inner periphery of the casting depending on the relative density compared to that of the melt. A one dimensional heat transfer model coupled with equation for force balance on particles is developed to predict the temperature distribution in the casting and mold regions, solidification time of the casting and particle segregation pattern in the casting region. The model takes into consideration the propagation of solidification front and movement of particles due to centrifugal acceleration which takes place either in the same or in opposite direction to that of the solidification front depending on the relative density difference between the particles and melt. In the force balance expression, repulsive force term is incorporated for the particles that are at the vicinity of the solid/liquid interface to calculate the particle segregation pattern in the casting region. The solution of the model equations has been obtained by *pure implicit finite volume technique* with modified variable time step (MVTS) approach.

The effects of various process parameters such as, rotational speed of the mold, size of the reinforcing material, relative density difference between the particle and melt, initial pouring temperature of the liquid melt, mold pre-heating temperature, heat transfer coefficient between the casting/mold interface are studied. It is noted that for a given set of operating conditions, the thickness of the particle rich region in the composite decreases with increase in rotational speed, particle size, relative density difference between the particle and melt, initial pouring temperature and initial mold temperature.
With decrease in the heat transfer coefficient between the casting/mold interface, the solidification time increases which, in turn, results in more intense segregation of solid particulates. Again, with increase in the initial volume fraction of the solid particulates, both the solidification time as well as the final thickness of the particulate rich region

increase. It is seen that, for *Al-Al_2O_3* and *Al-SiC* systems, depending upon the variables used in the investigation, up to certain distances from the outer periphery of the casting, the volume fraction of the particulates in the solidified composite remains the same as that of the initial melt for all the three particle sizes considered here. But for *Al-Gr* system, this behavior is seen only in case of 1 μm particle size, for a particular set of parameters investigated here.

LIST OF FIGURES:

LIST OF TABLES:

LIST OF SYMBOLS:

C	Specific heat, $J\,kg^{-1}\,K^{-1}$
h_1	Heat transfer co-efficient at $r = R_{oc}$, $W\,m^{-2}\,K^{-1}$
h_2	Heat transfer co-efficient at $r = R_{ic}$, $W\,m^{-2}\,K^{-1}$
h_3	Heat transfer co-efficient at $r = R_{om}$, $W\,m^{-2}\,K^{-1}$
h_4	Heat transfer co-efficient at $r = R_{og}$, $W\,m^{-2}\,K^{-1}$
H	Latent heat of solidification, $J\,kg^{-1}$
H_e	Effective latent heat of solidification, $J\,kg^{-1}$
k	Thermal conductivity, $W\,m^{-1}\,K^{-1}$
N	Rotational speed of the mold, *rpm*
R_e	Reynolds Number
R_{ic}	Position of the inner surface of the casting from center, *m*
R_{oc}	Position of the outer surface of the casting from center, *m*
R_{ig}	Position of the inner surface of the graphite mold from center, *m*
R_{og}	Position of the outer surface of the graphite mold from center, *m*
R_{im}	Position of the inner surface of the steel mold from center, *m*
R_{om}	Position of the outer surface of the steel mold from center, *m*
$R_{s(t)}$	Position of the solid-liquid interface from center, *m*
R_p	Particle radius, *m*
$r_o(t)$	Position of the particle at $t=0$, *m*
$r(t)$	Position of the particle at time t, *m*
$s(t)$	Thickness of the solidified casting as a function of time, *m*
T	Temperature, ^oC
T_f	Solidification front temperature, ^oC
T_L	Liquidus temperature of the base alloy, ^oC
T_S	Solidus temperature of the base alloy, ^oC
T_m	Temperature of the steel mold, ^oC

T_g	Temperature of the graphite mold, ^oC
T_{lc}	Temperature of the liquid region of the composite, ^oC
T_{sc}	Temperature of the solid region of the composite, ^oC
T_M	Initial temperature of the graphite and steel mold, ^oC
T_p	Pouring temperature, ^oC
T_α	Temperature of the ambient adjacent to the steel mold, ^oC
T_β	Temperature of the ambient adjacent to the casting inner surface, ^oC
t	Time, *secs*
Δt	Time increment, *secs*
V_r	Stokes velocity of the particles, $m\ s^{-1}$
V_s	Volume of solid particles in each segment, m^3
ρ_p	Density of the particle, $kg\ m^{-3}$
ρ_l	Density of the liquid, $kg\ m^{-3}$
α	Thermal diffusivity, $m^2\ s^{-1}$
ν	Viscosity of the base alloy, $N\ s\ m^{-2}$
ν_c	Apparent viscosity, $N\ s\ m^{-2}$
ω	Angular velocity of mold , $rad\ s^{-1}$
r	Particle position w.r.t. the center, m
$V_f(t)$	Volume fraction of particles in time t

Subscripts:

g	Graphite mold
m	Steel mold
ic	Position of the inner surface of the casting
oc	Position of the outer surface of the casting
ig	Position of the inner surface of the graphite mold
og	Position of the outer surface of the graphite mold
im	Position of the inner surface of the steel mold
om	Position of the outer surface of the steel mold
L	Liquid region of the base metal

S	Solid region of the base metal
lc	Liquid region of the composite
sc	Solid region of the composite

CHAPTER 1

INTRODUCTION:

1.1 INTRODUCTION:

Composites can be considered materials consisting of two or more chemically distinct constituents, on a macro scale, having a distinct interface separating them [1]. Properties of composites are strongly influenced by the properties of their constituent materials, their distribution, and the interaction between them. These materials have many advantages over conventional materials because of their superior performance in terms of strength, stiffness, toughness, high-temperature performance and other mechanical properties. Depending on the matrix materials, composites can be classified as polymer matrix composites, metal matrix composites and ceramic matrix composites.

Among this, metal matrix composites, where a strong ceramic reinforcement is incorporated into a metal matrix have proved to be an important class of materials, with the potential to replace a number of conventional materials being used in automotive, aerospace, defense, and leisure industries, where the demand for light weight and higher strength components is increasing. Metal matrix composites possess high levels of strength and stiffness, improved thermal stability, low coefficient of thermal expansion and improved wear and seizure resistance [2].

The functional gradient composite is a new type of composite that has become attractive because of its multi-functional properties, including the reinforced ceramic particle properties, matrix metal properties, and their combined properties [3]. These are designed to have heat resistant ceramics on their high temperature side and tough metal in their low temperature side, with a gradual compositional change. The main advantages of the functionally gradient composites are the gradual change of properties such as coefficient of thermal conductivity and electrical conductivity, thermal stress etc. resulting from the gradual distribution of its structure and reinforced phases, which can avoid the destruction caused by the properties mismatch at high temperature.

This thesis deals primarily with the functionally graded metal matrix composites where the reinforcement is in the form of ceramic powders such as alumina, silicon carbide and graphite in aluminium matrix.

1.2 DIFFERENT FABRICATION TECHNIQUES FOR THE PRODUCTION OF METAL MATRIX COMPOSITES:

Ceramic reinforced metal matrix composites can be prepared by both solid state (including powder metallurgy and diffusion bonding) and liquid state (squeeze casting, pressure infiltration, stirring casting, centrifugal casting etc) [3] processes. However, solid-state processing techniques require more time, costly equipments and often these are cumbersome. Compared to solid-state processing methods, liquid state processing (like casting techniques) are characterized by several advantages, i.e.,

- Lower production cost
- Time consumed is less
- Simple in operation
- Secondary processes are minimized
- Intricate shapes can be produced

Due to these advantages, liquid state processing techniques are becoming more popular.

1.2.1 FABRICATION TECHNIQUES OF FUNCTIONALLY GRADIENT COMPOSITES:

The fabrication of the functionally gradient composites has been accomplished via powder metallurgy (PM) techniques and deposition processes such as plasma spraying, physical vapor deposition (PVD), chemical vapor deposition (CVD), electro forming, and self – propagating high- temperature synthesis (SHS) [3]. Compositional

gradient is achieved by varying the chemistry of the powders and reactive gases with time in PM, PVD and CVD processes, respectively. But these processes are hard to be applied in practical use due to complex techniques and high cost. This has led to the development of an alternative technique. Centrifugal casting of metal matrix composites is an alternative technique to produce gradient composites very easily by controlling various process parameters according to the requirements.

1.3 CENTRIFUGAL CASTING OF METAL MATRIX COMPOSITES:

Centrifugal casting involves pouring liquid metal into a rapidly rotating mold, which may be mounted either vertically or horizontally, and continuing the rotation until solidification is complete. The main advantage of this technique is good mold filling combined with good micro structural control which usually gives excellent mechanical properties. During centrifugal casting of metal matrix composites, segregation of particles occurs due to centrifugal forces, either to the inner or to the outer part of the casting, depending on the relative densities of the particles and the melt, which results in particle reinforced functionally gradient composites [4-6]. The extent of segregation depends on various process parameters, such as geometry, pouring temperature, solidification time, density difference between the matrix and reinforced particles, rotational speed, etc.

1.4 REQUIREMENTS OF MATHEMATICAL MODELLING OF CENTRIFUGAL CASTING OF METAL MATRIX COMPOSITES:

During centrifugal casting of particles reinforced metal matrix composites, it is difficult to determine the temperature distribution and solidification time by experimental techniques. Because of this, accurate data on solidification time are not available. Estimation of solidification time and temperature distribution is a complex problem, because the moving ceramic particles disturb the temperature equilibrium. Also, the segregation of the particles alters the thermo-physical properties of composite melts during solidification. Therefore, it is desirable to estimate the solidification time and also influence of other processing parameters on the solidification time of metal matrix

composites through some alternate means. Mathematical modeling of the casting process based on heat and mass transfer analysis can be a useful alternate methodology.

1.5 BRIEF REVIEW OF MATHEMATICAL MODELLING OF CENTRIFUGAL CASTING OF METAL MATRIX COMPOSITES:

Kang and Rohatgi [7] have described the results of a heat transfer analysis of centrifugal casting of metal matrix composites by one-dimensional analysis considering the thermal mechanical properties due to particles moving as a function of temperature. These theoretical predictions have been compared with the results of Lajoye and Suery [8]. In their investigations, the positions of the dispersed particles at a given time have been analyzed as a first step. Then the temperature distributions in the mold and the solidifying metal have been analyzed at different time intervals and using these temperature distributions, solidification times for different centrifugal speeds, initial mold temperature, and pouring temperature of molten metal have been estimated. Siva Raju and Mehrotra [9] have presented a more realistic model where the volume fraction of the particles across the thickness of the casting varies with time. Siva Raju and Mehrotra have also considered variations in heat transfer coefficient and latent heat release.

1.6 OBJECTIVE:

The main objectives of the present investigation are as follows:

- To develop a model to describe the temperature distribution throughout the casting and mold regions, and particle segregation in the casting region. *Finite Volume Technique* has been used as the solution scheme unlike the finite difference method which was employed by Siva Raju and Mehrotra.
- Incorporation of repulsive force term in the force balance expression to calculate the particle segregation pattern in the casting region.
- To study the influence of different process parameters such as rotational speed of the mold, particle size, relative density difference between the particle and melt,

initial mold temperature, pouring temperature, heat transfer coefficient between the casting and mold on the solidification time of the casting and on the segregation pattern of the particles.

CHAPTER 2
MODEL FORMULATION:

Siva Raju and Mehrotra have presented a mathematical formulation based on one-dimensional heat transfer analysis incorporating variation in thermo-physical properties due to particle movement in the matrix. The present investigation is an attempt to further improve that analysis. At the outset, there are two principal differences between the present investigation and that of Siva Raju and Mehrotra.

1. Both Kang and Rohatgi [7] and Siva Raju and Mehrotra [9] in their models neglected the repulsive force term in their equations for force balance on particles. In the present investigations, the repulsive force which a particle experiences when it approaches a solid wall/solidification front is taken into consideration and characterized by an appropriate expression, the details of which are given in a later section of this chapter.
2. In the previous work of Siva Raju and Mehrotra, variation of volume fraction of particles with time is considered by ensuring conservation of total mass of particles at all times. In their work, the volume of particulates in between two consecutive nodal points always remain same. So, in that case the length of the segment varies with time and so are the nodes as they depend on constant volume fraction of particulates. But in the present formulation the nodes are fixed for all time and the variation of volume fraction of particles in any particular segment with time is calculated by taking into account the particle movement with time. One of the important features of the present model is the use of finite volume technique as the solution procedure unlike the finite difference scheme used in the previous work [10]. The advantage of finite volume method over finite difference one is the automatic conservation of all physical quantities unlike the approximation of so in the later case. The detailed description of the same is given in the 3rd chapter.

A schematic representation of the centrifugal casting of metal matrix composite, mathematically modeled in this investigation, is shown in Fig. 2.1. The

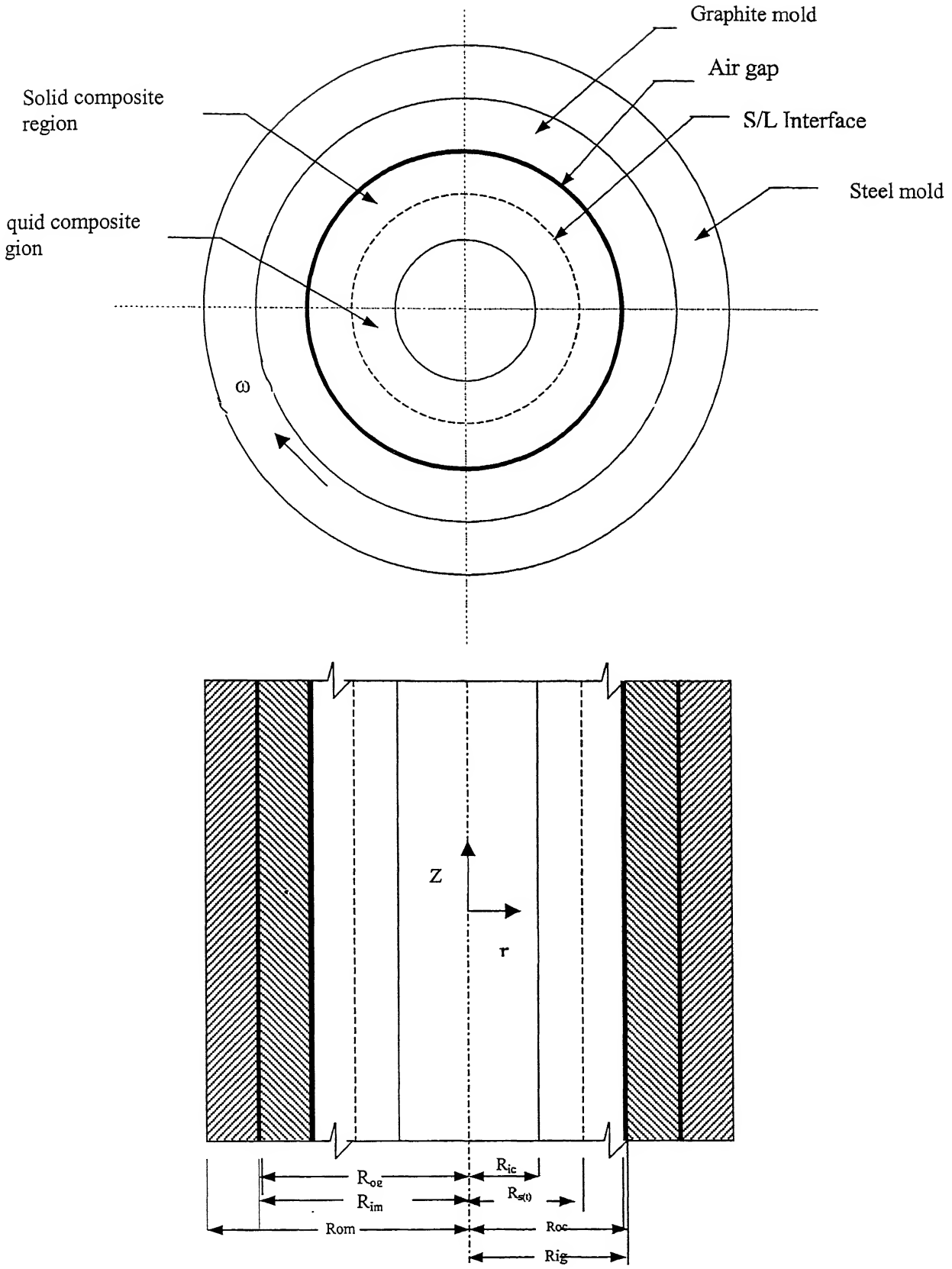

Figure 2.1: Schematic representation of the complete system of centrifugally cast metal matrix composites with particle segregation and solidification interface

heat is withdrawn from the liquid region of the casting, which is at temperature of T_{lc} , through the solidified composite region at temperature T_{sc}, to graphite mold at temperature T_g and subsequently through steel mold at temperature T_m to the surroundings. Heat is also radiated away from the inner surface of the casting. The dispersed particles in the liquid are at temperature T_{lc}. As the solidification proceeds by conduction of heat transfer through the composite to the graphite mold, the solid-liquid interface moves away from the graphite mold.

2.1 MODEL FORMULATIONS TO KNOW THE TEMPERATURE DISTRIBUTION IN CASTING AND MOLD REGION AND SEGREGATION PATTERN OF THE PARTICLES:

A mathematical model is formulated to predict the temperature distribution throughout the mold and casting regions and particle segregation within the liquid region of the casting.

The model is based on the following assumptions:

2.1.1 MODEL ASSUMPTIONS:

- The heat flow is purely one dimensional and perpendicular to the mold wall.
- The mold is filled with liquid metal containing solid particulates instantaneously, and that at the instant of mold filling the solid particulates are homogeneously distributed in the liquid metal matrix.
- Thermal properties of solid particulates and metal matrix are temperature invariant.
- Heat transfer co-efficient between casting and graphite mold decreases as solidification proceeds due to increase in air gap because of contraction of casting.
- Natural convection and movement of particles due to buoyancy are neglected.
- The interface position between solid and liquid regions is calculated by assuming it to be planar.

- There is no thermal resistance between particles and liquid metal.
- Reinforcement particles are assumed to be spherical in shape.
- The motion of the particles is stopped by the liquidus front, i.e. the particles do not move in the mushy zone of the casting and they are not rejected by the solidification front.
- For large volume fractions, interaction between particles occurs thus reducing their velocity. It is assumed that the reduction in velocity can be characterized by an increase of apparent viscosity of the liquid. The apparent viscosity can be represenied as [11]

$$\nu_c = \nu\ [1+ 2.5\ V_f(t) + 10.05\ V_f^2(t)] \qquad (2.1)$$

- Segregation of particles can only occur up to a maximum volume fraction equal to 52 % [12].

2.1.2 HEAT CONDUCTION FORMULATION:

This formulation is essentially the same as that of Kang and Rohatgi [7] and Siva Raju and Mehrotra [9].

2.1.2.1 Governing Equation:

The heat transfer processes in various regions of casting and mold are governed by one dimensional unsteady state heat conduction equation written in cylindrical co-ordinates.

$$\rho_i c_i \frac{\partial T_i}{\partial t} = \frac{1}{r}\frac{\partial}{\partial r}\left(rk_i \frac{\partial T_i}{\partial r}\right) \qquad (2.2)$$

where,

i = lc, sc, g, m for the liquid composite, solid composite, graphite and for steel mold regions, respectively.

k_{sc} , k_{lc} , c_{sc} , $c_{lc,}$ $\rho_{sc,}$ ρ_{lc} are estimated by determining the volume fractions of the solid particulates in the liquid and solid composite regions, which vary with time due to the movement of particles owing to the density difference between the liquid metal matrix and solid particulates.

2.1.2.2 Thermo-Physical Properties of Composites:

Thermal conductivities, densities and specific heats of composites in either liquid or solid regions are determined using the rule of mixtures described as follows as a function of volume fraction of particulate, $V_f(t)$ at any time 't' [13].

$$P_c = (1 - V_f(t))\, P_m + V_f(t) P_p \tag{2.3}$$

where, P_c refers to the property of composite under consideration, P_m and P_p are the corresponding properties of the matrix and particulates , respectively.
The volume fraction $V_f(t)$ depends on the viscosity of the alloy, particle size, mold rotational speed and the density difference between the particle and the molten metal.

2.1.2.3 Initial Conditions:

During centrifugal casting, before pouring the molten metal (which is at temperature T_p) into the mold, the mold is preheated to a certain temperature (T_M) to avoid the thermal damage to the mold. Therefore the initial temperature distribution (at time t=0) in the casting and mold regions considered as

$$T_{lc} = T_p \tag{2.4}$$

$$Tg = T_m = T_M \tag{2.5}$$

2.1.2.4 Boundary Conditions:

The boundary conditions in different regions of the casting and mold are as follows:

1. At the inner surface of the casting, i.e. , at $r = R_{ic}$

$$-k_{lc}\frac{\partial T_{lc}}{\partial r} = h_2(T_{ci} - T_{\beta}) \tag{2.6}$$

2. At the outer surface of the casting, i.e., at $r = R_{oc}$

$$-k_{sc}\frac{\partial T_{sc}}{\partial r} = h_1(T_{co} - Tgi) \tag{2.7}$$

3. At the inner surface of the graphite mold, i.e., at $r = R_{ig}$

$$-k_g\frac{\partial T_g}{\partial r} = h_1(T_{co} - T_{gi}) \tag{2.8}$$

4. At the outer surface of the graphite mold, i.e., at $r = R_{og}$

$$-k_g\frac{\partial T_g}{\partial r} = h_4(T_{go} - T_{mi}) \tag{2.9}$$

5. At the inner surface of the steel mold, i.e., at $r = R_{im}$

$$-k_m\frac{\partial T_m}{\partial r} = h_4(T_{go} - T_{mi}) \tag{2.10}$$

6. At the outer surface of the steel mold, i.e., at $r = R_{om}$

$$-k_m \frac{\partial T_m}{\partial r} = h_3 (T_{mo} - T_\alpha) \tag{2.11}$$

7. At solid-liquid interface, i.e., at $r = R_{s(t)}$

$$T_{sc} = T_{lc} = T_f \tag{2.12}$$

8. The energy balance at solid-liquid interface, i.e., at $r = R_{s(t)}$ is obtained by equating the rate of heat removed from the solid phase in the positive r direction to the sum of rate off heat supplied to the interface from the liquid phase in the positive r direction and rate of heat liberated at the interface during solidification, i.e.

$$-k_{sc} \frac{\partial T_{sc}}{\partial r} = -k_{lc} \frac{\partial T_{lc}}{\partial r} + \rho_{sc} H \frac{\partial s(t)}{\partial t} \tag{2.13}$$

2.1.2.5 Formulation of Heat Transfer Co-Efficient:

The rate of solidification of the liquid composite is significantly dependent upon the air gap formed at the casting-graphite mold interface due to contraction of the casting as well as thermal expansion of the mold during solidification, and also to some extent on the air gap at graphite–steel mold interface due to imperfect contact. It is assumed that the heat transfer coefficient between casting and graphite mold due to air gap varies as [8].

$$h_1 = h_i \left(\frac{h_f}{h_i} \right)^{\frac{s(t)}{r_i}} \tag{2.14}$$

where h_i is initial heat transfer coefficient, h_f is final heat transfer coefficient, $s(t)$ is solidified thickness and r_i is total thickness of the casting.

2.1.3 FORCE BALANCE ON PARTICLES:

Here it has been assumed that fluid is under laminar flow ($R_e \leq 1$). So, the force balance equation is as follows:

$$\frac{4}{3}\pi R_p^3(\rho_p - \rho_l)\omega^2 r - 6\pi\nu R_p V_r = \frac{4}{3}\pi R_p^3 \rho_p \frac{dV_r}{dt}$$

Under zero acceleration, the velocity of the spherical particle according to Stokes law is

$$V_r = \frac{4R_p^2 \Delta\rho\omega^2 r}{18\nu} \tag{2.15}$$

where, R_p is radius of the particle, ω is angular velocity, r is particle position, ν is viscosity of the melt and $\Delta\rho = \rho_p - \rho_l$ i.e., density difference between the particle (ρ_p) and liquid metal (ρ_l) .The Reynolds number is given by

$$R_e = \left| \frac{\rho_l V_r 2R_p}{\nu} \right| \tag{2.16}$$

During vertical centrifugal casting, a particle which is suspended in the liquid is subjected to a vertical acceleration due to gravity g and a centrifugal acceleration $\gamma = \omega^2 r$. Generally γ is much greater than g which allows the vertical displacement of the particle to be ignored. Therefore the different forces on a particle are

- Centrifugal force due to the rotation
- Viscous force due to drag effect
- Repulsive force due to movement of solid-liquid interface

A schematic representation of the various forces acting on the particle is given in Fig. 2.2.

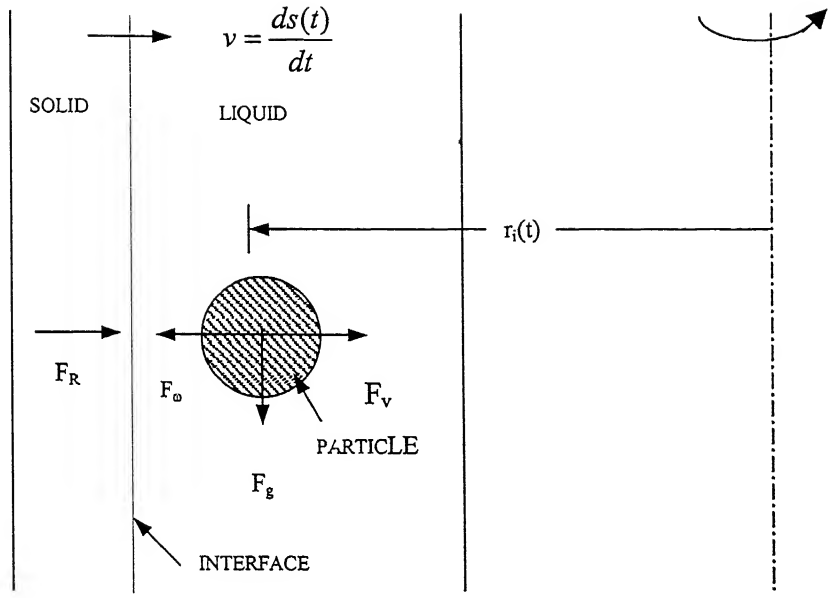

Figure 2.2: Schematic diagram of various forces acting on a moving particle in the liquid melt

The force balance equation on the particle due to centrifugal, viscous, and repulsive forces can be expressed as [14]

$$F_\omega - F_v - F_R = F_{net} \tag{2.17}$$

where, F_{net} is the net force on the particle, F_ω is the force due to centrifugal acceleration, F_v is viscous force, and F_R is the repulsive force. It is to be noted that the repulsive force is significant only on those particles which are in the vicinity of a solid wall or the solid-liquid interface. Hence, the force balance for the particles which are far away from the solid-liquid interface can be written as follows.

$$F_\omega - F_v = F_{net} \tag{2.18}$$

$$\frac{4}{3}\pi R_p^3(\rho_p - \rho_l)\omega^2 r - 6\pi v R_p \frac{dr}{dt} = \frac{4}{3}\pi R_p^3 \rho_p \frac{d^2 r}{dt^2} \tag{2.19}$$

Solution of Eq. (2. 19) for a particle moving at a constant velocity, gives its position at any instant of time t as

$$r(t) = r_0 \exp\left[\frac{4\omega^2(\rho_p - \rho_l)R_p^2 t}{18v}\right] \tag{2.20}$$

where $r_o(t)$ is the position of the particle at time $t=0$

2.1.3.1 Repulsive Force :

2.1.3.1.1. Importance of the use of repulsive force term:

In the present work of centrifugal casting of metal matrix composites, the final distribution of the second phase in the solidified material is important for obtaining the

requisite properties, hence an understanding of the phenomena which contribute to the redistribution of the particles during solidification is very important in order to achieve the desired results.

When the solidification front of an alloy approaches a particle in the melt, interactions take place between them due to three main reasons: the molecular surface forces between the particles and the front, distortion of the temperature field because of the different thermal properties of the particle and distortion of the solute concentration field due to blocking of solute diffusion from the front by the particle. If the molecular surface forces are repulsive, the front can push the particles along with it unless the repulsive force is overcome by the viscous drag on the particle [15]. Several theories have been proposed which are based on the concept of molecular surface forces repelling the particle from the growth front and thus facilitating the entry of liquid into the gap between the growing solid and the particle [16-18]. The magnitude of the forces depend on the dimensions of the gap between the particle and the front and hence on the morphology of the front. When a liquid containing a dispersion of particles is solidified, the solidification front can exert a repulsive force on the particles and push them along with it, thereby increasing the particle concentration in the last solidifying liquid. The pushing of the particle is considered as a steady state phenomenon in which the particle and the solidification front move with the same velocity and the gap width is maintained constant.

2.1.3.1.2. Proposed Theories for the Expression of Repulsive Force:

Several models explaining the concept of repulsive force or wall effect on the particle or individual have been developed when the laters enter into the influence zone of the wall or solid surface.

. The model proposed by Sasikumar and Kumar [19] demonstrates a system consisting of silicon carbide particles dispersed in Aluminium melt, solidified vertically from the bottom as well as in cylindrical molds. They have explained the effect of repulsive force on the particle exerted by the solidification front. It has also been known that the phenomenon of particle pushing occurs only below a certain velocity of the

advancing solidification front known as the critical velocity. If the velocity of the growth front is greater than the critical velocity, the particle is engulfed by the front. The critical velocity is a function of the particle size, the temperature gradient at the solidification front, and a number of material properties like the ratio of thermal conductivities of the particle and the melt, the co-efficient of molecular surface forces between the particle and the solidification front, etc. In this method for calculating the critical velocity, the first step is the calculation of the change in shape of the solidification front as it approaches the particle. From this, the dimensions of the gap between the particle and the front are calculated. The repulsive force exerted on the particle depend on the gap and these are calculated and balanced to obtain the velocity of the particle.

$$V_p = \frac{F_R}{12\pi\eta \int_0^{r_p} r dr \int_r^{r_p} \frac{\rho d\rho}{h^3(\rho)}} \tag{2.21}$$

where,

$$F_R = 2\pi B \int_0^{r_p} \frac{r dr}{h^3(r)} \tag{2.22}$$

r_p = Radius of the particle

$h(r)$ = The gap between the particle and the front

B = The co-efficient for molecular interaction between the front and the particle

η = Viscosity of the melt

The maximum velocity under which steady state is possible is identified as the critical velocity. Numerically this is determined by calculating the V_p at different distances, L of the solidification front from the particle. As L decreases, V_p increases and then goes through a maximum. It is concluded from this that if the solidification front were to have a velocity, V, equal to $V_p(L)$, steady state pushing of the particle occurs when the front is at a distance L from the particle. If the V were to exceed the maximum possible value for V_p then no steady state pushing is possible; the gap between the particle and the front

continues to decrease and the particle is engulfed by the front. The maximum value of V_p is therefore identified as the critical velocity.

Sannomiya and Matuda [20] has proposed a model which describes the behavior of fish in a water tank where the wall exerts the repulsive force on the individual when it approaches towards it. The detailed description of this model is given in the later section of this chapter.

In this thesis, the expression of the repulsive force that is exerted by the solidification front on the particle is taken from the mathematical model that described by Sannomiya and Matuda [20].

2.1.3.1.3. Reasons in support of the use of the same expression of the repulsive force in the case of a particle:

As fish is a living being, its movement is influenced by several factors such as, its velocity relative to the ambient water, the extent of swimming forward continuously according to its swimming ability, interaction among the individuals, the character of uniforming the swimming speed and the direction in the school, repulsion and attraction from the walls when the individual approaches towards it closely. The forces which describe all these activities are damping force, propulsive force, interactive force, schooling force, repulsive and attractive force from the wall respectively [20].

As fish is a living species, when it approaches the wall, it avoids to strike against the same which is a psychological phenomenon happening to all living beings. But in the case of solidification of a liquid containing a dispersion of second phase particles, when the later reaches the solidification front, they do not re-bounce (due to the involvement of no psychological phenomenon and the assumption that there is no rejection of particles by the solidification front). The velocity of the particles slow down in the influence zone of the wall due to wall effect and finally they get absorbed by the solidification front.. As repulsive force is independent of the tank shape and size [21], so the parameters estimated by Sannomiya and Matuda is used in the present thesis.

2.1.3.1.4 Expression for repulsive force :

For the particles which are in the vicinity of a solid surface or the solid-liquid interface, the expression of the repulsive force is [20]

$$F_R = k_w^+ \sum_{l=1}^{L} f_{wil^+} \tag{2.23}$$

$$f_{wil^+} = \begin{cases} v_{il} \dfrac{d^+ - d_{il}}{d^+} e_l & for v_{il} > 0 and d_{il} < d^+ \\ 0 & otherwise \end{cases} \tag{2.24}$$

where k_w^+ is a constant co-efficient .

L is the number of wall sides.

d^+ is the width of the influence zone of the wall ($\approx 10^{-6}$ cm) [22]

d_{il} is the distance from the individual i to the wall l.

the unit vector e_l is normal to the wall.

For the individual i, v_{il} is the velocity component normal to the wall l.

So, particle position at any given instant of time is given by

$$r(t) = r_0 \exp\left[\frac{4/3\pi\omega^2(\rho_p - \rho_l)R_p^3 t}{K + 6\pi\nu Rp}\right] \tag{2.25}$$

where, $K = k_{w^+}\left(\dfrac{d^+ - d_{il}}{d^+}\right)$ (2.26)

2.1.3.1.5 Estimation of k_w^+ by Sannomiya and Matuda:

In the work of Sannomiya and Matuda, an individual fish is assumed to be a particle. The depth of water in the tank where experiment has been carried out is shallow and the motion of fish is restricted within a two-dimensional space. Since only a small school is considered, the motion of each fish is described individually by a state equation. The experiment used to start with releasing the fish into a specific position of the tank and the motion of fish is restricted within a two-dimensional space. As a general rule, the fish school swims along the wall. The image of the fish behavior used to be recorded during ten minutes by a video tape recorder. The image data was sampled at intervals of 0.5secs to obtain the time series data. Since only a small school has been considered , the motion of each fish is described individually by a state equation. The parameters included in the equation are identical irrespective of the individual, under the assumption that fish in a school are homogeneous. When an individual approaches a wall closely, it avoids striking against the wall. Repulsive force expresses such a behavior. Sannomiya and Matuda have estimated the value of k_w^+ by using the observation data of this water tank experiment and by applying the least squares algorithm. The validity is investigated by testing the whiteness of the residual of the state equation and also by comparing the simulation result with those of the experimental ones.

2.1.4 DETERMINATION OF VOLUME FRACTION :

In order to determine the volume fraction variation in liquid metal matrix, the casting thickness is divided into n equal segments. Nodal points are considered as the extreme positions of each segment. The volume fraction of particulates in a particular segment is defined as the ratio of volume of particles to the total volume of that segment. This is given as:

$$V_{fs} = \frac{V_s}{V_s + V_l} = \frac{1}{1 + \frac{\rho_{sml}}{\rho_{lms}}} \tag{2.27}$$

where V_{fs} is the volume fraction of the particulates, V_s is the volume of reinforced particles, and V_l is the volume of the metal matrix in each segment. Since the initial volume fraction of the particulates is known in each segment, the volumes and masses of the solid particles and matrix melt can be obtained using the following relationships.

$$V_s = V_{fs}\, V$$
$$V_l = V - V_s \tag{2.28}$$

$$m_s = V_s \rho_s$$
$$m_l = V_l \rho_l \tag{2.29}$$

where V is total volume of each segment, m_s is mass of solid in each segment, and m_l is total mass of liquid in each segment.

For simplicity, initially the particle positions are considered at the nodal points at time $t=0$. The particles at different nodal points have different velocities, because the motion of each particle in the liquid melt is dependent on its position. The total number of particulates in the casting region always remains the same. The new particle positions for time $t+\Delta t$ are obtained by using either Eq. (2.20) or (2.25) taking into account the appropriate conditions. The new particles may fall either on any node or in the interior of any volume segment. From this, the total number of particulates in any volume segment can be found out and thus, the new volume of the particulates in each segment can be calculated. The volume of each segment remains fixed for all time. So from this, the new volume fraction of the particulates per unit length can be obtained for time $t+\Delta t$. To calculate the particle position for the next time step, initial positions of the particulates are updated with the new particle positions that have already obtained and further calculations are carried out in the similar manner.

CHAPTER 3

SOLUTION PROCEDURE:

The model equations have been solved numerically by using simple implicit finite volume technique. For this the " r - t " domain is subdivided into small intervals of constant Δr in space and variable Δt in time as shown in Fig. 3.1. The variable time step approach is used to solve the problem. This approach requires that at each time level t_n the time step Δt_n is so chosen that the interface moves exactly a distance Δr during the time interval Δt, hence always stays on the node. Therefore, the problem is mainly concerned with the determination of the time step $\Delta t = t_{n+1} - t_n$ such that in the time interval from t_n to t_{n+1}, the interface moves from the position $n\Delta r$ to the next position $(n+1)\Delta r$ [23].

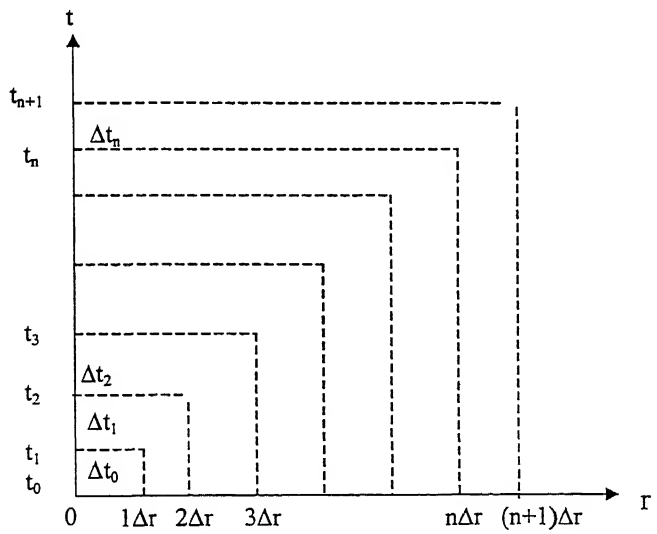

Figure 3.1: Subdivision of " r-t " domain using constant Δr , variable Δt

3.1 ADVANTAGES OF FVM OVER FDM :

The usual procedure for deriving *finite-difference equations*, consists of approximating the derivatives in the differential equation via a truncated Taylor series. The method includes the assumption that the variation of the dependent variable is somewhat like a polynomial in the independent variable, so that the higher derivatives are unimportant. This assumption, however, leads to an undesirable formulation when, exponential variations are encountered. The Taylor-series formulation is relatively straight-forward but allows less flexibility and provides little insight into the physical meanings of the terms [24].

But, the basic idea of *finite volume formulation* lends itself to direct physical interpretation. Here, the calculation domain is divided into a number of non-overlapping control volumes such that there is one control volume surrounding each grid point. The differential equation is integrated over each control volume. Piecewise profiles expressing the variations of the dependent variable between the grid points are used to evaluate the required integrals. The result is the discretization equation containing the values of dependent variables for a group of grid points. The discretization equation obtained in this manner expresses the conservation principle for the dependent variable for the finite control volume, just as the differential equation expresses it for an infinitesimal control volume. The most attractive feature of the control-volume formulation is that the resulting solution would imply that the integral conservation of quantities such as mass, momentum, and energy is exactly satisfied over any group of control volumes and, of course, over the whole calculation domain. This characterstic exists for any number of grid points, not just in a limiting sense when the number of grid points becomes large. Thus, even the coarse-grid solution exhibits exact integral balances [24,25].

3.2 VALIDATION OF FINITE VOLUME TECHNIQUE:

The validation of this technique has been carried out by comparing the numerical solutions with those of the analytical ones in determining the temperature profiles for various cases. Figures 3.2 and 3.3 show the comparison between the analytical and numerical techniques for unsteady-state heat conduction in a slab and cylinder of finite thicknesses, where the initial temperatures are given and surface temperatures are fixed [26-29] and Fig. 3.4 shows the validation of this technique for the steady state temperature profiles in the case of a finite hollow cylinder where temperature is fixed at one boundary and the other boundary is a convective one. The analytical solution for Fig. 3.4 is as follows:

$$\left[1+\frac{hr_1}{k}\ln\left(\frac{r_2}{r}\right)\right]T = T_2 + \frac{hr_1}{k}T_f \ln\left(\frac{r_2}{r}\right) \tag{3.1}$$

where,

T_2 = Temperature of the outer surface of the cylinder, i.e., at $r = r_2$

T_f = Temperature of the ambient adjacent to the inner surface of the cylinder

h = Heat transfer coefficient at the inner surface of casting

k = Thermal conductivity of the cylinder

r = Distance from the axis of the cylinder

3.3 FINITE VOLUME APPROXIMATION:

The differential equation and the boundary conditions for both the mold and casting regions can be discretized by using implicit method. The thickness of each mold region is subdivided into n equal grids. The number of grids in the solid and liquid

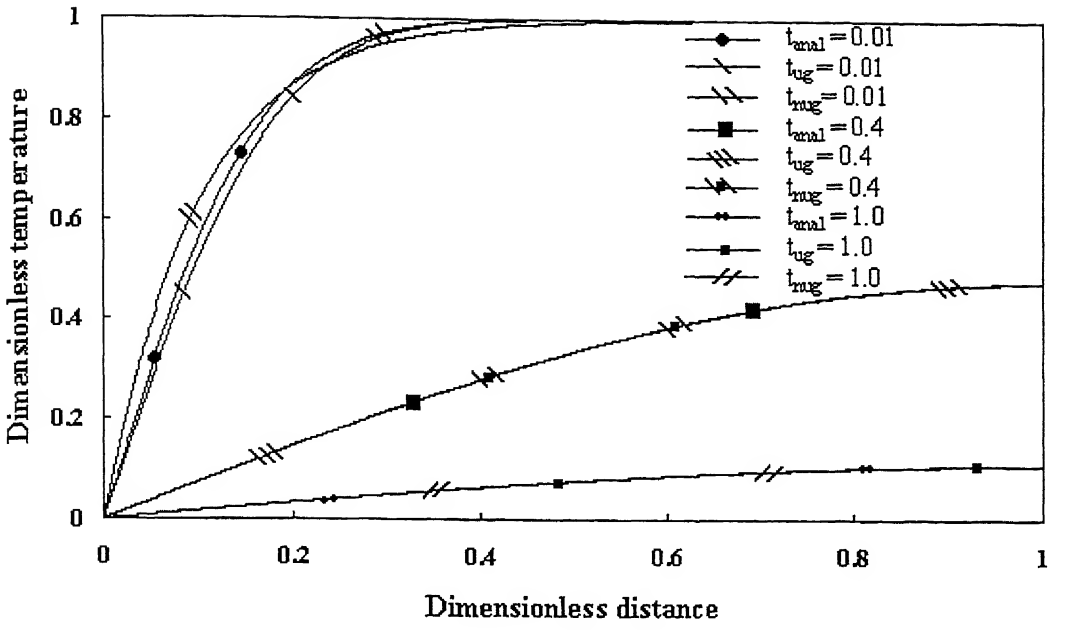

Figure 3.2: Temperature profiles for unsteady-state heat conduction in a slab of finite Thickness

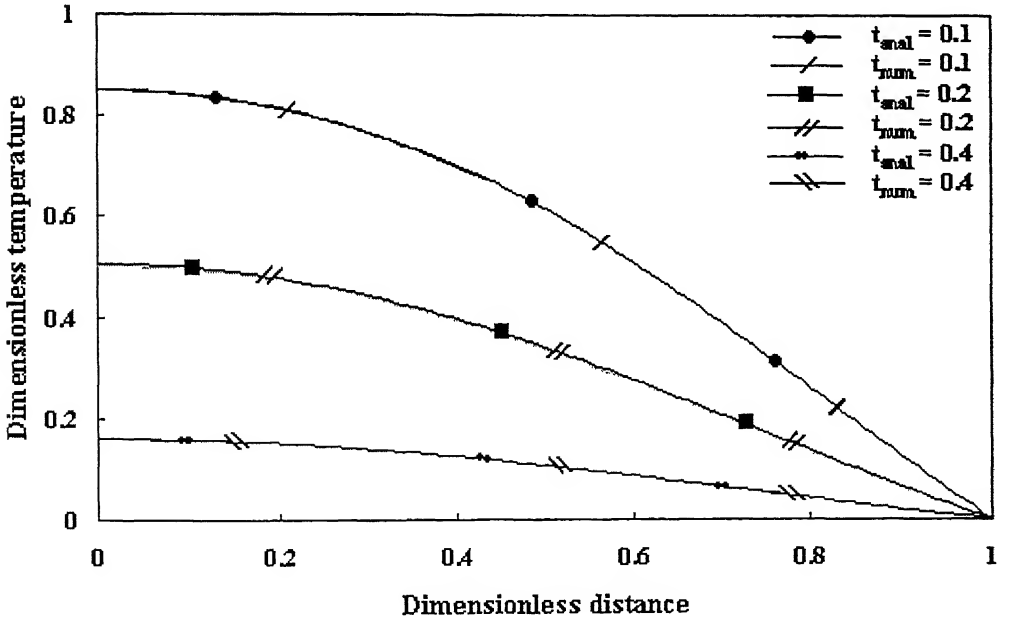

Figure 3.3: Temperature profiles for unsteady-state heat conduction in a cylinder of finite Thickness

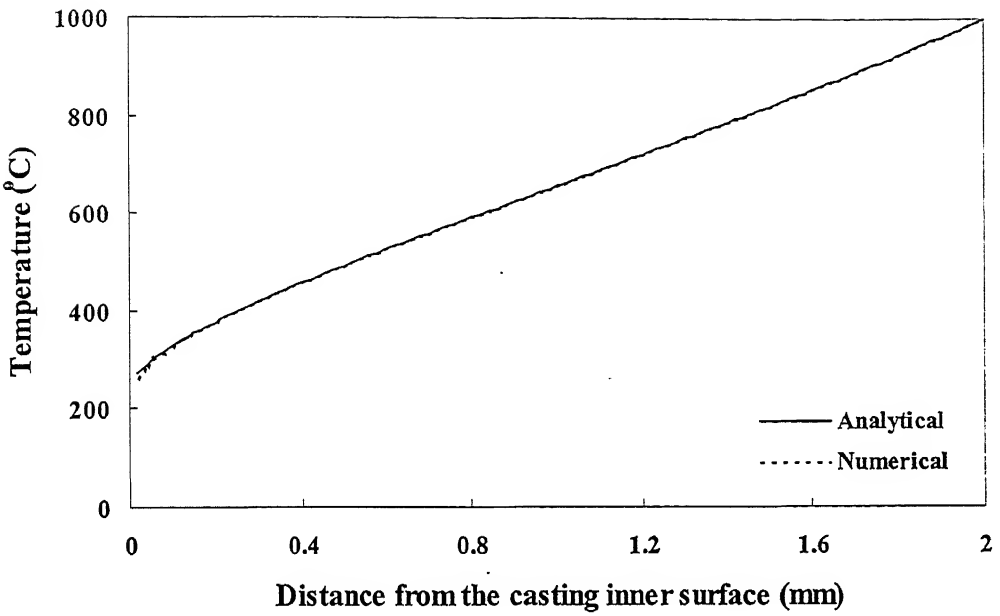

Figure 3.4: Temperature profiles for steady-state heat conduction in a cylinder of finite thickness

composite regions vary with time. It means that for the solid composite region the number of grids (n_i) goes on increasing as the solidification proceeds, and for the liquid composite region, the number of grids (n-n_i) decreases, but their sum always remains same as n.

Equation (2.2) is solved with boundary conditions Eqs. (2.6) through (2.12) using pure implicit finite volume technique. The resultant discretized equations are arranged in a tri-diagonol matrix form and the solution of these equations is obtained by using Thomas Algorithm (TDMA) which gives temperature distribution in both casting and mold regions for a particular time step Δt_n. The detailed description is presented in section 3.5 of the present chapter.

3.4 DETERMINATION OF TIME STEPS:

During solidification, the interface moves from the position $n\Delta r$ to the position $(n+1)\Delta r$ within a time interval of $\Delta t_i = t_{i+1} - t_i$, which is not known in a priori.
Using modified variable time step (MVTS) method, the actual value of Δt_i is obtained by iteration as follows [30].

1. An initial guess value for the time step Δt_i is chosen as $\Delta t_i = \Delta t_i^{(0)}$.
2.Using $\Delta t_i^{(0)}$, the nodal temperatures are obtained by solving the finite volume equations for the mold and casting regions.
3. Then the time step $\Delta t_i^{(1)}$ is obtained by using the estimated temperatures in step (2) in Eq. (3.13).
4. Using $\Delta t_i^{(1)}$, the steps (2) and (3) are repeated to obtain $\Delta t_i^{(2)}$.
5. Iteration is carried out until the difference between the two consecutive time steps satisfies a specified convergence criterion.
6. To obtain Δt_{i+1}, $\Delta t_{i+1}^{(0)i} = \Delta t_i$ is assumed and the steps from (2) to (5) are repeated.
7. The steps from (2) to (6) are repeated till the solid-liquid interface reaches the inner surface of the casting.

3.5 DISCRETIZATION OF THE GDE AND BOUNDARY CONDITIONS ACCORDING TO THE CONTROL VOLUME TECHNIQUE:

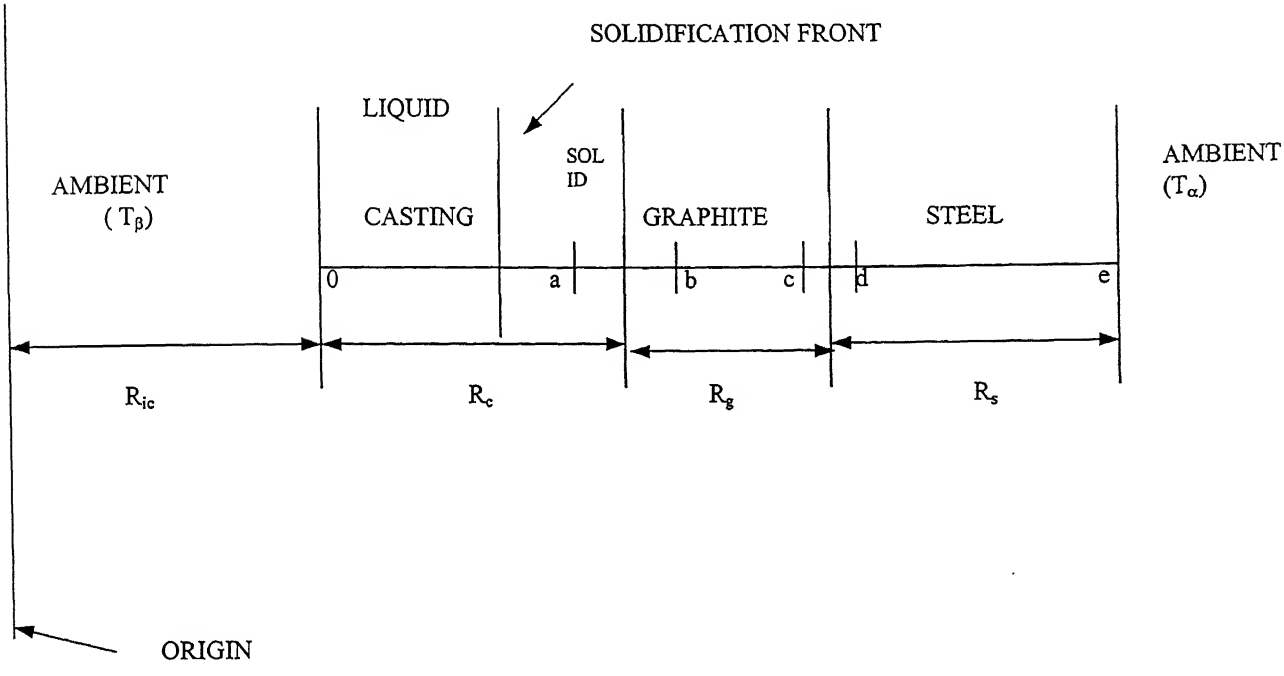

Figure 3.5: Schematic diagram showing different nodal points of the casting and mold Region

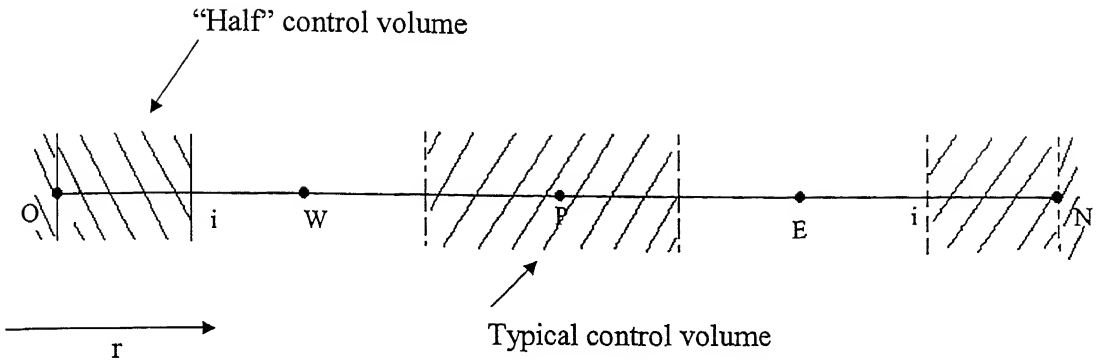

Figure 3.6: Control volumes for the internal and boundary points

FOR ALL INTERNAL POINTS:

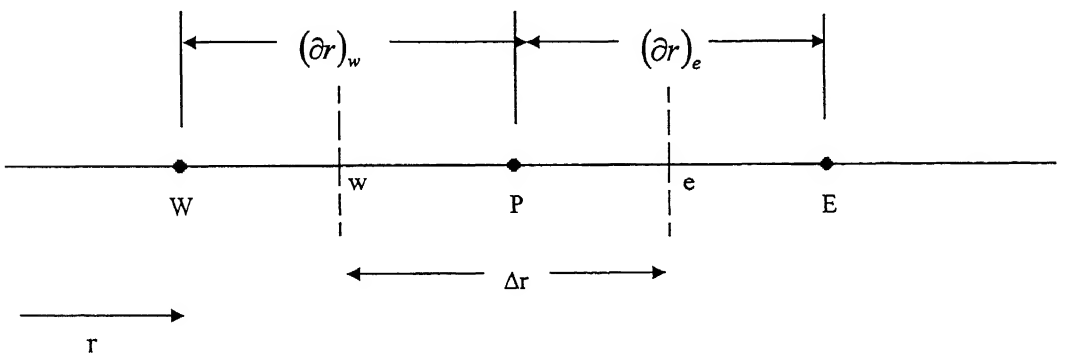

Figure 3.7: Grid- point cluster for the one-dimensional problem

The differential equation (2.2) is integrated over the full control volume as follows:

$$\int_w^e \int_t^{t+\Delta t} r\rho c \frac{\partial T}{\partial t} dt dr = \int_t^{t+\Delta t} \int_w^e \frac{\partial}{\partial r}\left(rk \frac{\partial T}{\partial r}\right) dr dt \tag{3.2}$$

Then the discretized form of Eq. (3.2) becomes:

$$\left[\left(\frac{r_e^2 \rho_e c_e - r_w^2 \rho_w c_w}{2\partial t}\right) + \left(\frac{r_e k_e}{(\partial r)_e}\right) + \left(\frac{r_w k_w}{(\partial r)_w}\right)\right] T_P = \left(\frac{r_e k_e}{(\partial r)_e}\right) T_E + \left(\frac{r_w k_w}{(\partial r)_w}\right) T_W + \left(\frac{r_e^2 \rho_e c_e - r_w^2 \rho_w c_w}{2\partial t}\right) T_P^o \tag{3.3}$$

FOR INNER SURFACE OF THE CASTING (NODE '0'):

Integrating the differential equation (2.2) over half control volume:

$$\int_0^i \int_t^{t+\Delta t} r\rho c \frac{\partial T}{\partial t} dt dr = \int_t^{t+\Delta t} \int_0^i \frac{\partial}{\partial r}\left(rk \frac{\partial T}{\partial r}\right) dr dt \tag{3.4}$$

and substituting the boundary condition [Eq. (2.6)], the discretized equation becomes:

$$\left[\left(\frac{\rho_i c_i r_i^2 - \rho_0 c_0 r_0^2}{2\partial t}\right) + \left(\frac{r_i k_i}{\partial r}\right) + (r_0 h_2)\right] T_0 = \left(\frac{r_i k_i}{\partial r}\right) T_1 + (r_0 h_2) T_\beta + \left(\frac{\rho_i c_i r_i^2 - \rho_0 c_0 r_0^2}{2\partial t}\right) T_0^o \tag{3.5}$$

where,

$$k_i = \left(\frac{2k_1 k_0}{k_1 + k_0}\right) \tag{3.6}$$

k_1 = thermal conductivity of node '1'

k_0= thermal conductivity of node '0'

FOR NODE 'a':

Integrating the governing equation (2.2) over the full control volume and using the boundary condition [Eq. (2.7)], the discretized equation becomes:

$$\left[\left(\rho c \partial r \frac{(r_e + r_w)}{2\partial t}\right) + \left(\frac{r_e k_e h_1}{2k_{sc}}\right) + \left(\frac{r_w k_w}{(\partial r)_w}\right)\right] T_a = \left(\frac{r_e k_e h_1}{2k_{sc}}\right) T_{a+1} + \left(\frac{r_w k_w}{(\partial r)_w}\right) T_{a-1} + \left(\rho c \partial r \frac{(r_e + r_w)}{2\partial t}\right) T_a^o \tag{3.7}$$

FOR NODE 'b':

Integrating the governing equation (2.2) over the full control volume and using the boundary condition [Eq. (2.8)], the discretized equation becomes:

$$\left[\left(\rho c \partial r \frac{(r_e + r_w)}{2\partial t}\right) + \left(\frac{r_e k_e}{(\partial r)_g}\right) + \left(\frac{r_w k_w h_1}{2k_g}\right)\right] T_b = \left(\frac{r_e k_e}{(\partial r)_g}\right) T_{b+1} + \left(\frac{r_w k_w h_1}{2k_g}\right) T_{b-1} + \left(\rho c \partial r \frac{(r_e + r_w)}{2\partial t}\right) T_b^o \tag{3.8}$$

FOR NODE 'c':

Integrating the governing equation (2.2) over the full control volume and using the boundary condition [Eq. (2.9)], the discretized equation becomes:

$$\left[\left(\rho c \partial r \frac{(r_e + r_w)}{2\partial t}\right) + \left(\frac{r_e k_e h_4}{2k_g}\right) + \left(\frac{r_w k_w}{(\partial r)_w}\right)\right] T_c = \left(\frac{r_e k_e h_4}{2k_g}\right) T_{c+1} + \left(\frac{r_w k_w}{(\partial r)_w}\right) T_{c-1} + \left(\rho c \partial r \frac{(r_e + r_w)}{2\partial t}\right) T_c^o \tag{3.9}$$

FOR NODE 'd':

Integrating the governing Eq. (2.2) over the full control volume and using the boundary condition [Eq. (2.10)], the discretization equation becomes:

$$\left[\left(\rho c \partial r \frac{(r_e + r_w)}{2\partial t}\right) + \left(\frac{r_e k_e}{(\partial r)_s}\right) + \left(\frac{r_w k_w h_4}{2k_s}\right)\right] T_d = \left(\frac{r_e k_e}{(\partial r)_s}\right) T_{d+1} + \left(\frac{r_w k_w h_4}{2k_s}\right) T_d + \left(\rho c \partial r \frac{(r_e + r_w)}{2\partial t}\right) T_d^o$$

(3.10)

FOR OUTER SURFACE OF THE STEEL MOLD (NODE 'e'):

Integrating the governing equation (2.2) over the half control volume:

$$\int_i^e \int_t^{t+\Delta t} r\rho c \frac{\partial T}{\partial t} dt dr = \int_t^{t+\Delta t} \int_i^e \frac{\partial}{\partial r}\left(rk \frac{\partial T}{\partial r}\right) dr dt \qquad (3.11)$$

and using the boundary condition [Eq. (2.11)] , the discretized equation becomes:

$$\left[\left(\frac{\rho_e c_e r_e^2 - \rho_i c_i r_i^2}{2\partial t}\right) + \left(\frac{r_i k_i}{\partial r}\right) + (r_n h_3)\right] T_e = \left(\frac{r_i k_i}{\partial r}\right) T_{e-1} + (r_i h_3) T_\alpha + \left(\frac{\rho_e c_e r_e^2 - \rho_i c_i r_i^2}{2\partial t}\right) T_e^o$$

(3.12)

At Solid-Liquid Interface:

Equation (2.12) represents the condition of continuity of temperature at the interface, i.e.:

$$T_{sc} = T_{lc} = T_f \qquad (3.13)$$

The time required to move the solidification front from one node to the other can be derived from the Eq. (2.13) as follows:

$$\Delta t = \frac{\rho_{sc} H_e \Delta s(t)}{k_{lc}\left(\frac{\partial T_{lc}}{\partial r}\right)_i - k_{sc}\left(\frac{\partial T_{sc}}{\partial r}\right)_i} \tag{3.14}$$

Temperature profile for all the internal points, when the solidification front moves from one node to the other, is shown in Fig. 3.7. So, the time required to move the solidification front from one node to the other for all internal points is given as:

$$\Delta t = \frac{\rho_{sc} H_e \Delta s(t)}{k_{lc_i}\left(\frac{T_{lc} - T_f}{(\partial r)_c}\right) - k_{sc_i}\left(\frac{T_{sc} - T_f}{(\partial r)_c}\right)} \tag{3.15}$$

When the solidification front moves to the last node, i.e., node adjacent to the ambient, then time required is:

$$\Delta t = \frac{\rho_{sc} H_e \Delta s(t)}{h_2\left(T_0 - T_\beta\right) - k_{sc_i}\left(\frac{T_{sc} - T_f}{(\partial r)_c}\right)} \tag{3.16}$$

and the temperature profile is shown in Fig. 3.8.

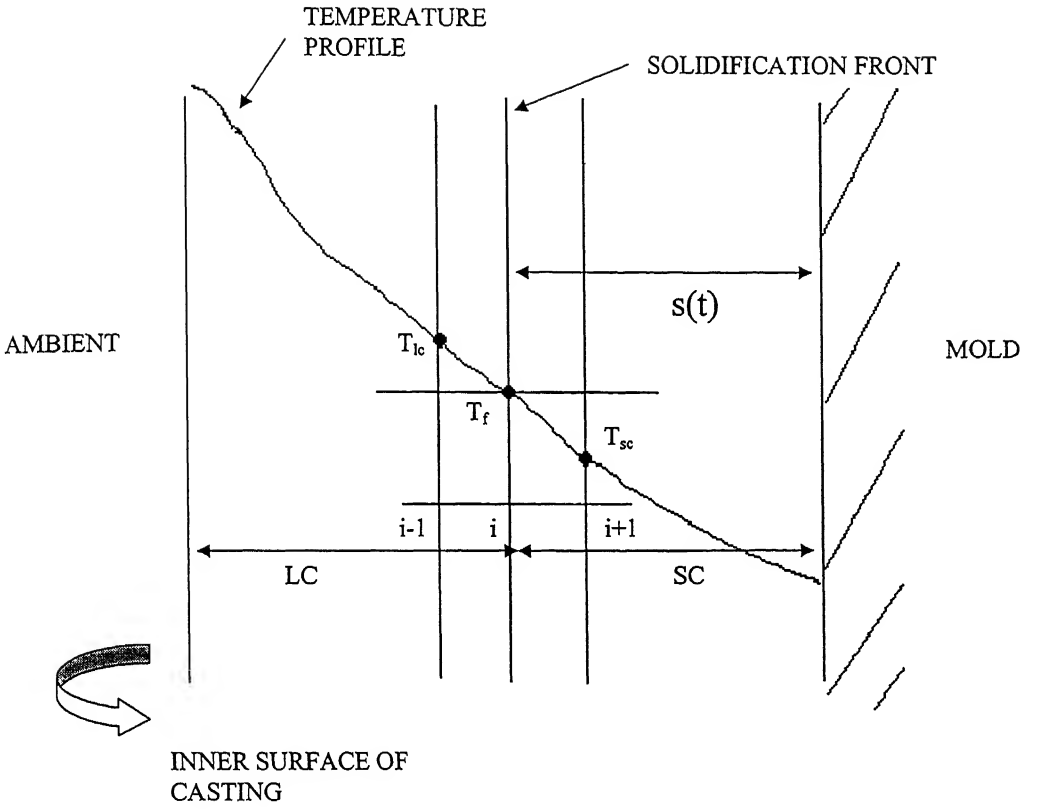

Figure 3.7: Schematic diagram of the temperature profile for all internal points

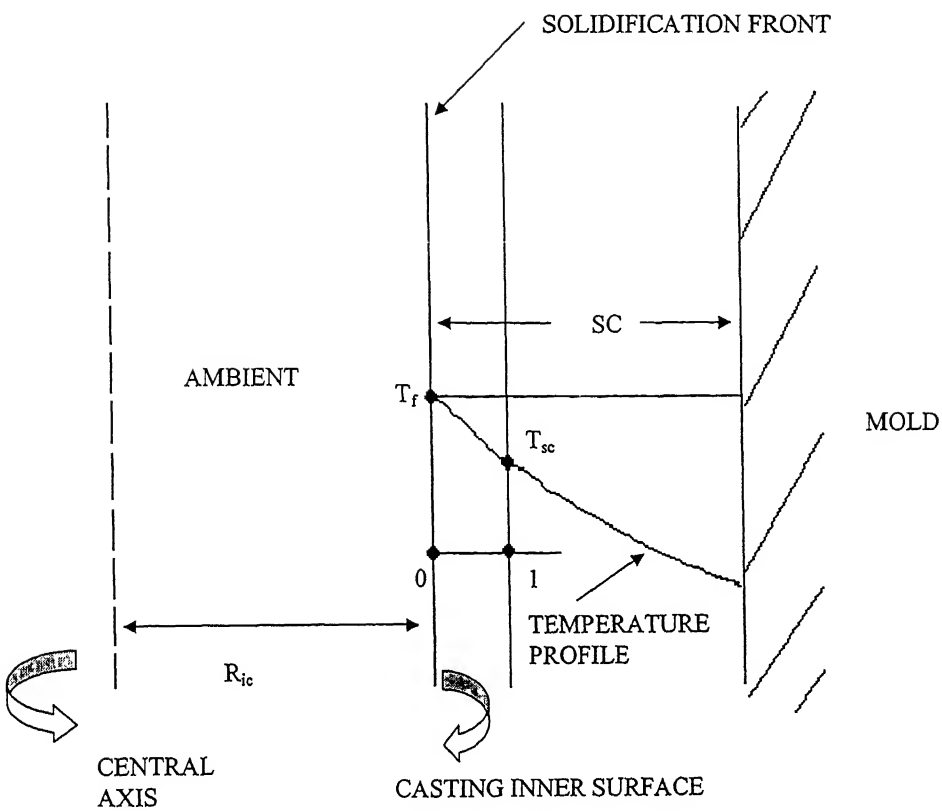

Figure 3.8: Schematic diagram of the temperature profile when the solidification front moves to the node adjacent to the ambient

Equations (3.3), (3.5), (3.7), (3.8), (3.9), (3.10), (3.12), (3.13) are arranged in the tri-diagonal matrix form and the solution of these equations is obtained by using the Thomas Algorithm (TDMA). This results in temperature distribution in both the casting and mold regions for a particular time step Δt.

3.6 SEGREGATION OF PARTICLES:

During centrifugal casting, segregation of particles takes place in the liquid composite due to the movement of particles resulting from difference in densities of the particles and the melt, and also due to centrifugal acceleration. By solving Eqs. (2.27) and (2.28) using the appropriate equations from Eqs. (2.20) and (2.25) through Eq. (2.1) the thickness of the particle-rich region is estimated for various rotational speeds of the mold at various times. The particle movement is neglected in the mushy zone of the casting, which is characterized by the temperature region ($T_s \leq T \leq T_L$), because on this zone the viscosity, ν_c, sharply increases.

CHAPTER 4

RESULTS AND DISCUSSIONS:

In this thesis, the model equations are solved to evaluate the followings for various operating conditions.

i. Particle segregation pattern
ii. Solidification time
iii. Temperature distribution in the casting and mold region

The parameters examined are:

i. Rotational speed of the mold
ii. Size of the reinforcing material
iii. Relative density difference between the matrix and reinforcing material
iv. Heat transfer co-efficient between the casting/mold interface
v. Initial pouring temperature of the liquid melt
vi. Initial mold temperature
vii. Initial volume fraction of the particulates in the melt

Thermo-physical properties of the matrix metal, reinforcement materials, graphite and steel molds used in this simulation are given in Table 4.1 [31,32]. Various design and operating parameters, like geometric constants for the casting and the mold, the heat transfer coefficients at different regions of the casting and the mold, and initial temperatures of the mold and metal used in the simulation are given in Table 4.2 [7,33]. The cooling conditions at the inner surface of the casting and at the outer surface of the steel mold are defined in terms of the heat transfer co-efficient h_2, h_3 respectively and the heat transfer due to the air gap at the metal-mold interface is characterized by h_1. Since the actual values of h_1 are not known, computations have been carried out for a wide range of values from 1000 to 10000 $W/m^2/K$ for this co-efficient. The results of this simulation are presented in the following sections.

Table 4.1: Thermo-physical properties of matrix metal, reinforcement particles, and mold materials [31,32]

Thermo-physical Properties	*Aluminium (A356)*	Al_2O_3	*SiC*	*Graphite*	*Carbon Steel Mold*	*Graphite Mold*
$k\ (W\,m^{-1}\,K^{-1})$	159	24	24	38	57.8	38
$\rho\ (kg\,m^{-3})$	2685	4000	3200	1900	7800	1900
$C\ (J\,kg^{-1}\,K^{-1})$	963	600	690	710	481	710
$T_S\ (^{o}C)$	555	-	-	-	-	-
$T_L\ (^{o}C)$	615	-	-	-	-	-
$T_f\ (^{o}C)$	555	-	-	-	-	-
$H\ (K\,J\,kg^{-1})$	389	-	-	-	-	-
$\nu\ (N\,s\,m^{-2})$	0.002	-	-	-	-	-

Table 4.2: Design & operating parameters used in simulation [7,33]

Outer diameter of steel mold, D_{om} *(mm)*	215.0
Outer diameter of graphite mold, D_{og} *(mm)*	150.0
Outer diameter of casting, D_{oc} *(mm)*	100.0
Inner diameter of casting, D_{ic} *(mm)*	80.8
Initial heat transfer co-efficient due to air gap at the metal-mold interface, h_i $(W m^{-2} K^{-1})$	1000 to 10000
Heat transfer co-efficient at the inner surface of casting, h_2 $(W m^{-2} K^{-1})$	8.4
Heat transfer co-efficient at the outer surface of steel mold, h_3 $(W m^{-2} K^{-1})$	8.4
Heat transfer co-efficient between the graphite-steel mold interface, h_4 $(W m^{-2} K^{-1})$	10000
Initial Pouring temperature of liquid metal, T_p $(^{\circ}C)$	650,730,800
Initial mold temperature, T_M $(^{\circ}C)$	200,250,300
Speed of rotation, *N (rpm)*	1000,1500,2000
Particle size, R_p (μm)	1,2,3
Ratio of initial to final heat transfer co-efficient, $\frac{h_i}{h_f}$	10

4.1 CALCULATION OF PARTICLE SEGREGATION PATTERN:

The results of this simulation are presented in the form of

i. Volume fraction of the particles

ii. Thickness of the particle rich region for the entire region of the casting

4.1.1 Effect of Rotational Speed of the Mold:

Figures 4.1 and 4.2 show the effect of rotational speed of the mold on the segregation pattern of the particles, i.e., on the thickness of the particle rich region. The various rotational speeds used in these simulations are 1000,1500 and 2000 rpm respectively. Figure 4.1 is for the condition where the reinforcement particles are heavier than the liquid melt and Fig. 4.2 is for where the matrix metal is heavier than the reinforcing particles. From these two figures it is evident that, thickness of the particle segregated region decreases with increase in the rotational speed of the mold, i.e., more denser segregation pattern is observed with higher rotational speed. This is because, increase in rotational speed of the mold increases the centrifugal acceleration, which subsequently increases the centrifugal force on the particles. Depending upon the relative density difference between the particles and the matrix melt, and whether it is positive or negative, the particles move with a greater velocity towards the outer or inner periphery of the casting and get segregated there. It is observed in Fig. 4.1 that, there is a horizontal portion near the outer periphery of the casting which signifies that the final volume fraction of the particulates in the solidified composite is equal to that of the initial volume fraction in the melt, before reaching the maximum in the segregation pattern and this horizontal portion decreases with increase in the rotational speed of the mold. The reason is, rate of solidification is very fast at the beginning, which is more than the particle velocity due to which the particles are not able to move towards the casting/mold interface leading to the volume fraction of the particulates in the solidified composite same as that of the initial volume fractions up to certain distances from the outer periphery. Gradually as the solidification front moves to the interior of the casting, time

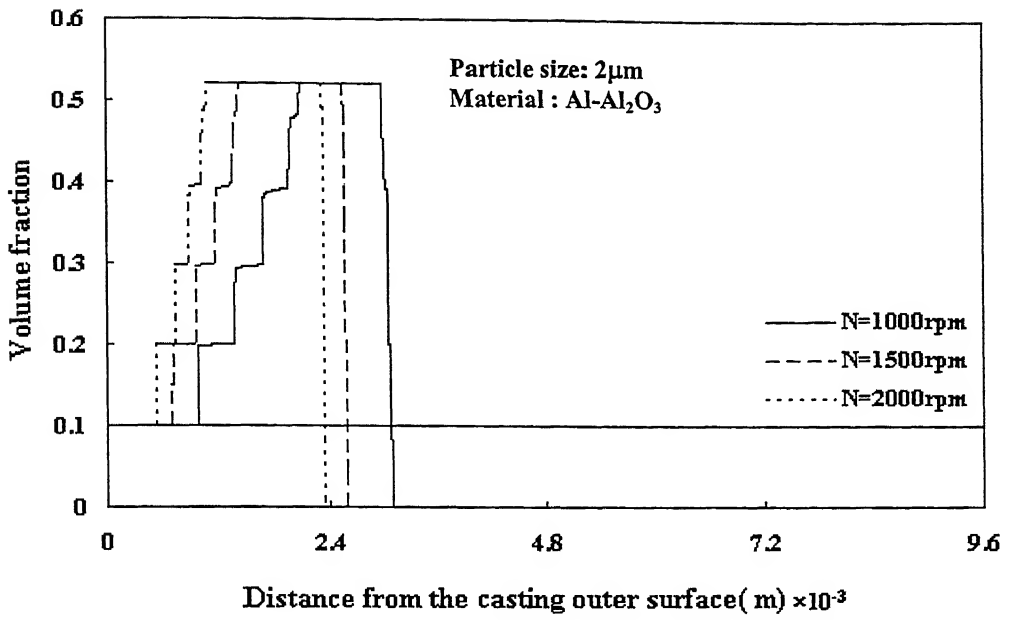

Figure 4.1: Effect of rotational speed of casting on particle segregation pattern after complete solidification for $\rho_p > \rho_l$

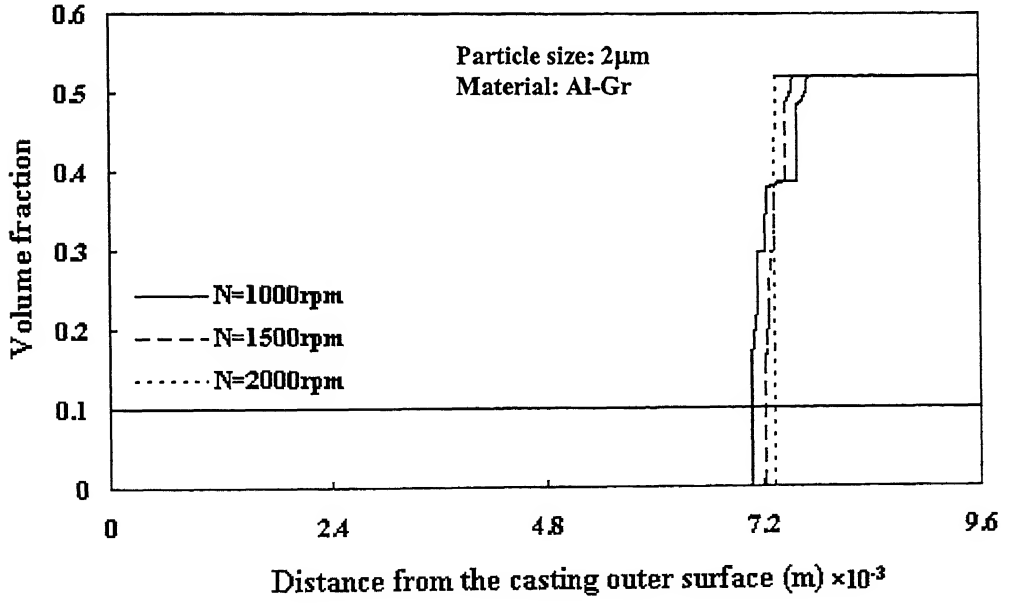

Figure 4.2: Effect of rotational speed of casting on particle segregation pattern after complete solidification for $\rho_p < \rho_l$

required to solidify a volume segment having the same dimension increases, as a result of which particles get more time to move towards the outer periphery of the casting leading to a segregated region next to the horizontal pattern. But with increase in the rotational speed of the mold, the centrifugal force on the particles increases and after certain time the velocity of the particles due to the centrifugal force becomes more than the velocity of the solidification front leading to less horizontal portion in the case of higher rotational speed. It is observed that, the thickness of the horizontal portion in case of *Al- Al_2O_3* decreases from 9.73×10^{-4} to 5.21×10^{-4} m when the rotational speed increases from 1000 to 2000 rpm. For Figure 4.2, particles get sufficient time to move to the inner surface of the casting, which leads to a maximum segregation at the inner periphery of the casting. The thickness of the Al_2O_3 rich region varies from 3.085×10^{-3} to 2.337×10^{-3} m, while that of graphite rich region varies from 2.301×10^{-3} to 2.128×10^{-3} m as the rotational speed increases from 1000 to 2000 rpm after complete solidification, as shown in Figs. 4.1 and 4.2.

4.1.2 Effect of Particle Size:

Figures 4.3 and 4.4 show the effect of particle size on the thickness of the particle rich region, for three different particle sizes, namely 1, 2 and 3 μm. Figure 4.3 is the case where the density of the particle is more than that of the matrix material and Fig. 4.4 is the case where the density of the particle is less than that of the liquid melt. From these two figures it is evident that, the thickness of the particle rich region decreases with increase in particle size leading to more intense particle segregation. With increase in particle size, both the centrifugal and viscous forces increase, but the increase in centrifugal force is more than that of the viscous force. Hence, larger particles move rapidly towards the outer or inner periphery of the casting depending upon the relative density difference between the particle and the liquid melt and form more intense segregation. In Fig. 4.3, the horizontal nature of the segregation pattern decreases with increase in the particle size. This is because, larger the particle size, larger will be its momentum. As a result, particles with greater momentum move faster than the rate of solidification front so penetrate into the melt to a farther distance than the particles of

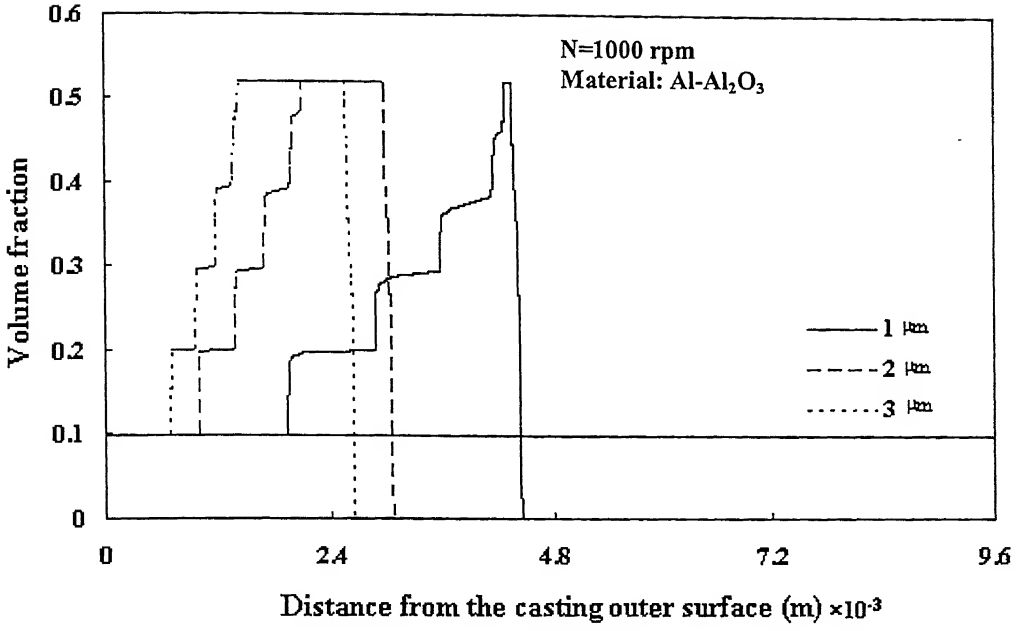

Figure 4.3: Effect of particle size on particle segregation pattern after complete solidification for $\rho_p > \rho_l$

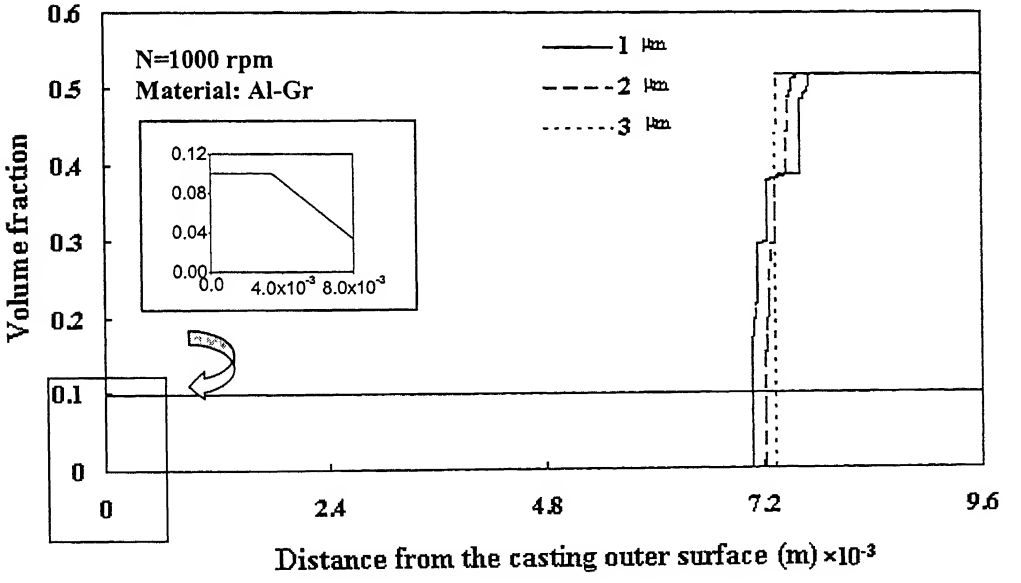

Figure 4.4: Effect of particle size on particle segregation pattern after complete solidification for $\rho_p < \rho_l$

smaller size. It is observed that, the thickness of the horizontal portion in case of *Al-Al_2O_3* decreases from 1.933×10^{-3} to 6.85×10^{-4} m when the particle size increases from 1 to 3 μm. In *Al-Gr* system, for 1 μm particle size the volume fraction of the particles in the solidified composite, in the volume segment just adjacent to the casting/mold interface remains the same as that of the initial volume fraction in the melt unlike to that of 2 and 3 μm particle size. The distance of this horizontal region from the casting/mold interface is 3.4273×10^{-6} m. The reason is, with increase in particle size, centrifugal force on the particle increases and larger particles move with higher velocity towards the inner periphery and do not get trapped by the solidification front near the outer periphery of the casting. But in case of 1 μm particle size, the velocity of the particles in volume segment adjacent to the casting/mold interface is lesser than the velocity of the solidification front which results in trapping of the particles within the solidifying layer. As a result, in this volume segment the volume fraction of the particulates in composite is the same as that of the initial melt. The thickness of the Al_2O_3 rich region varies from 4.449×10^{-3} to 2.639×10^{-3} m, while that of graphite rich region varies from 2.519×10^{-3} to 2.259×10^{-3} m as the particle size increases from 1 to 3 μm after complete solidification, as shown in Figs. 4.3 and 4.4.

4.1.3 Effect of Relative Density Difference Between the Particle and melt:

Figure 4.5 shows the effect of relative density difference between the particles and the melt on the thickness of the particle rich region for the case where the density of the particle is more than that of the melt. It is seen that the thickness of the particle rich region decreases with increase in the relative density difference between the particle and the melt. The reason that with increase in the relative density difference between the particle and the melt, the net centrifugal force on the particle increases due to which the particles travel to a farther distance leading to more intense particle segregation. As the particulate density decreases from 4000 kg/m^3 (Al_2O_3) to 3200 kg/m^3 (SiC), the thickness of the particle segregated region increases from 2.989×10^{-3} to 4.003×10^{-3} m.

4.1.4 Effect of Initial Pouring Temperature:

Figures 4.6 to 4.8 show the effect of initial pouring temperature of the liquid melt on the particle segregation pattern for three different particle sizes, namely 1, 2 and 3 μm. The three different values of T_p considered are, 650, 730 and 800 ^oC. All other parameters are kept fixed in these simulations. Figure 4.9 is a plot of variation of thickness of the particle rich region with initial pouring temperature for different particle sizes. It is observed that with increase in initial pouring temperature, the thickness of the particle rich region decreases for all the three particle sizes that are considered. Higher initial pouring temperature essentially means that the larger amount of heat is to be removed from the melt before solidification begins. Hence, the metal matrix composites takes longer time to solidify and during this extra time the reinforcement particles are able to segregate more forming a denser segregation pattern.

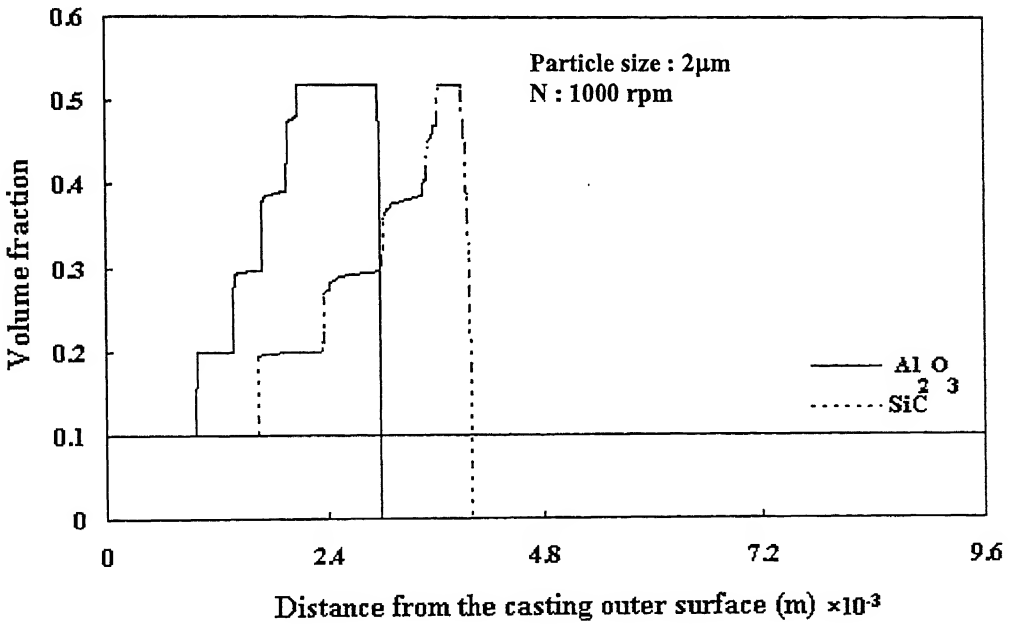

Figure 4.5: Effect of relative density difference between the reinforcement material and the melt on particle segregation pattern after complete solidification

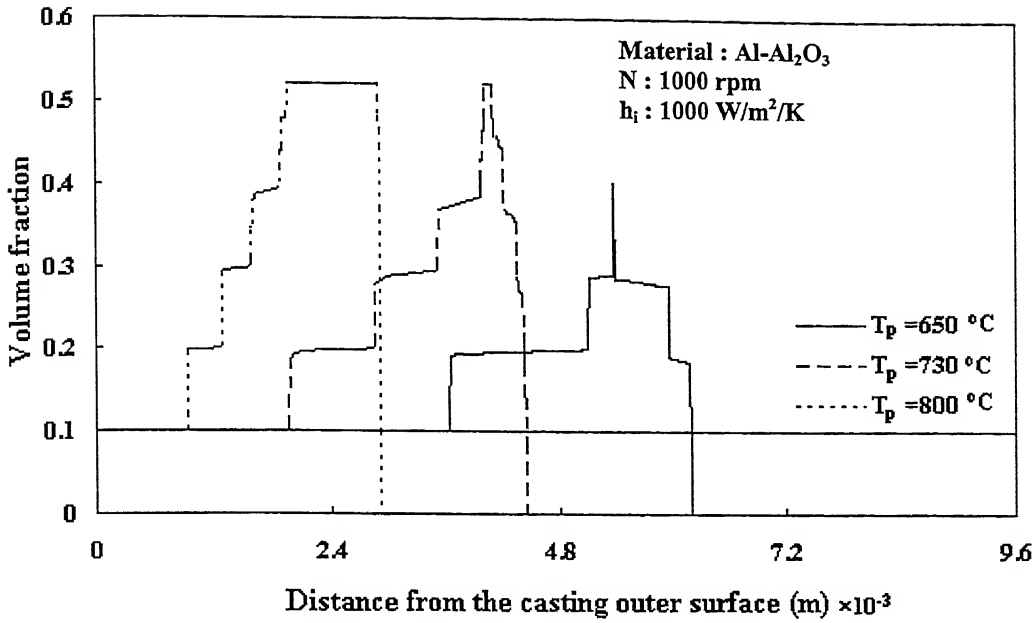

Figure 4.6: Effect of pouring temperature on the particle segregation pattern for 1μm particle size

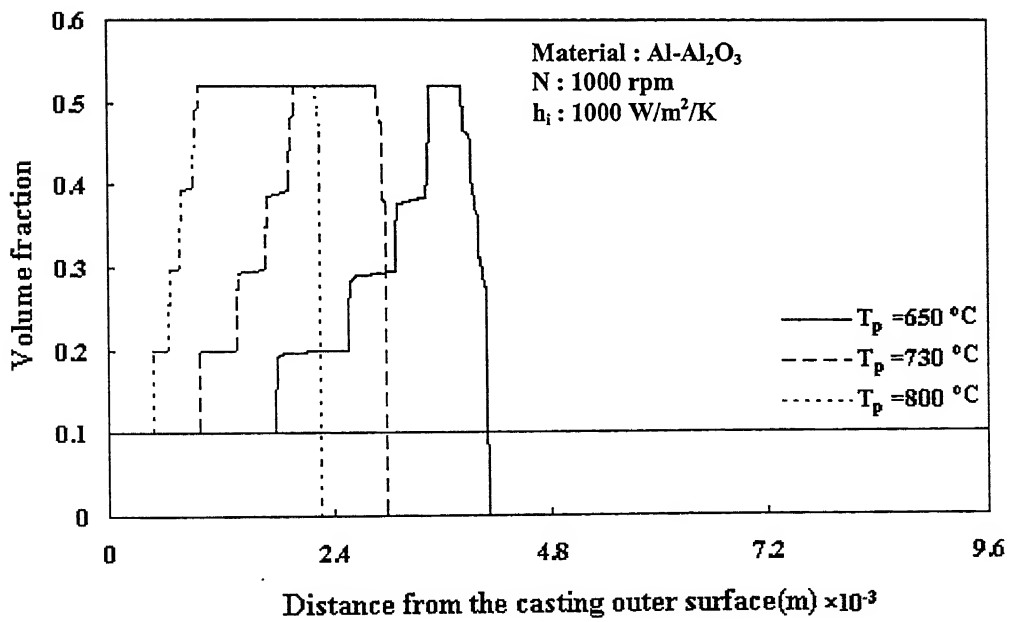

Figure 4.7: Effect of pouring temperature on the particle segregation pattern for 2μm particle size

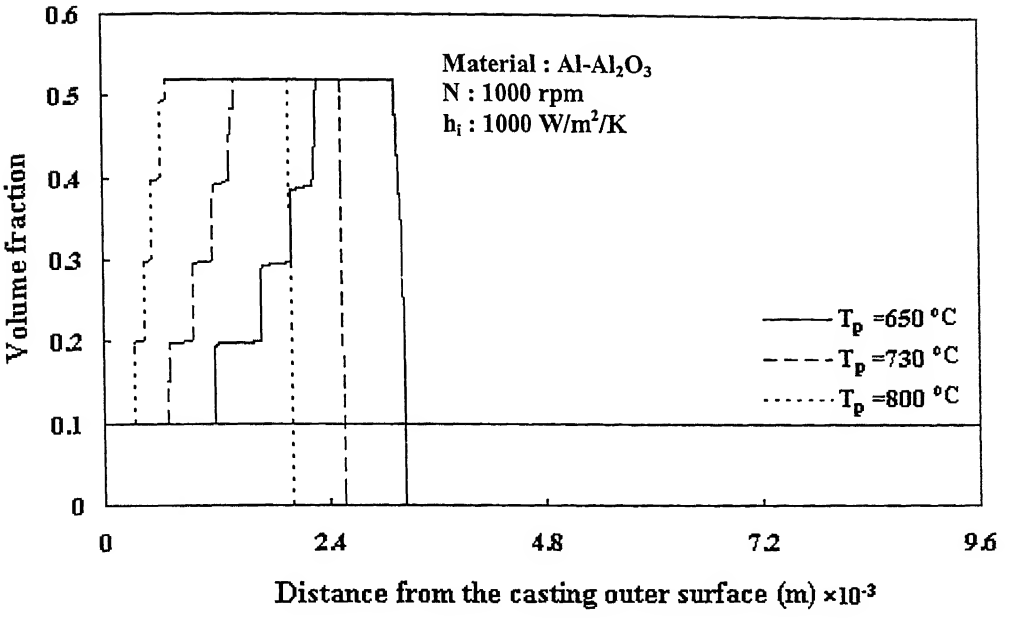

Figure 4.8: Effect of pouring temperature on the particle segregation pattern for $3\mu m$ particle size

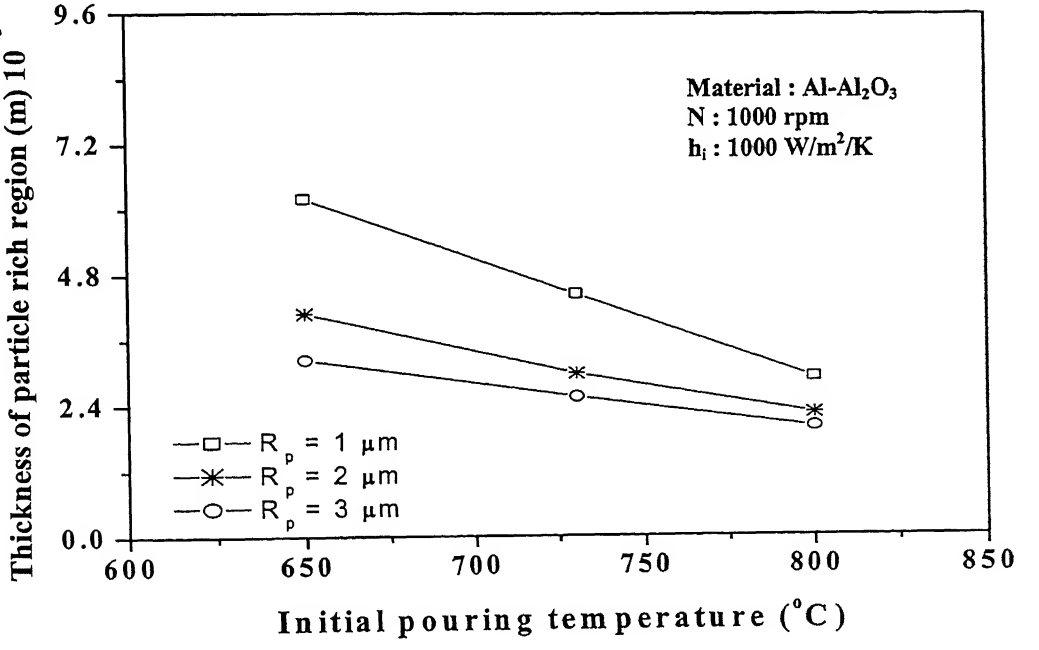

Figure 4.9: Influence of initial pouring temperature (T_p) on the variation of thickness of particle rich region of $Al\text{-}Al_2O_3$ composite

4.1.5 Effect of Initial Mold Temperature:

Figures 4.10 to 4.12 show the effect of initial mold temperature on the particle segregation pattern for three different values of T_M, namely 200, 250 and 300 ^oC and for three different particle sizes, viz 1, 2 and 3 μm. All the other parameters are kept fixed. Figure 4.13 is a plot of thickness of the particle rich region verses the initial mold temperature for the three different particle sizes. It is observed that with increase in initial mold temperature, the thickness of the particle rich region decreases as in the previous case. Higher initial mold temperature essentially means, reduced thermal gradient between the melt and the mold resulting in reduced heat transfer between them. Hence, the metal matrix composites take longer time to solidify and during this extra time the reinforcement particles are able to segregate more.

4.1.6 Effect of Heat Transfer Co-efficient at the Metal/Mold Interface:

Figures 4.14 to 4.16 show the effect of heat transfer coefficient at the metal/mold interface on the segregation pattern of the particles. It is seen that the thickness of the particle rich region increases with increase in heat transfer coefficient between the metal and the mold. This is because the rate of heat transfer is directly proportional to the heat transfer coefficient at the metal/mold interface. Higher the heat transfer coefficient at this interface, higher is the rate of heat transfer. Thus reduces the solidification time of the metal matrix and leads to an increase in particle rich region because the particles do not get enough time for more intense segregation and therefore remain distributed in the larger region of the composite.

4.1.7 Effect of Particulate Volume Fraction:

Figure 4.17 shows the effect of initial volume fraction of the particulates on the final distribution of the particles in the solidified composite and also on the thickness of the particulate rich region. It is evident from the figure that the thickness of the particle

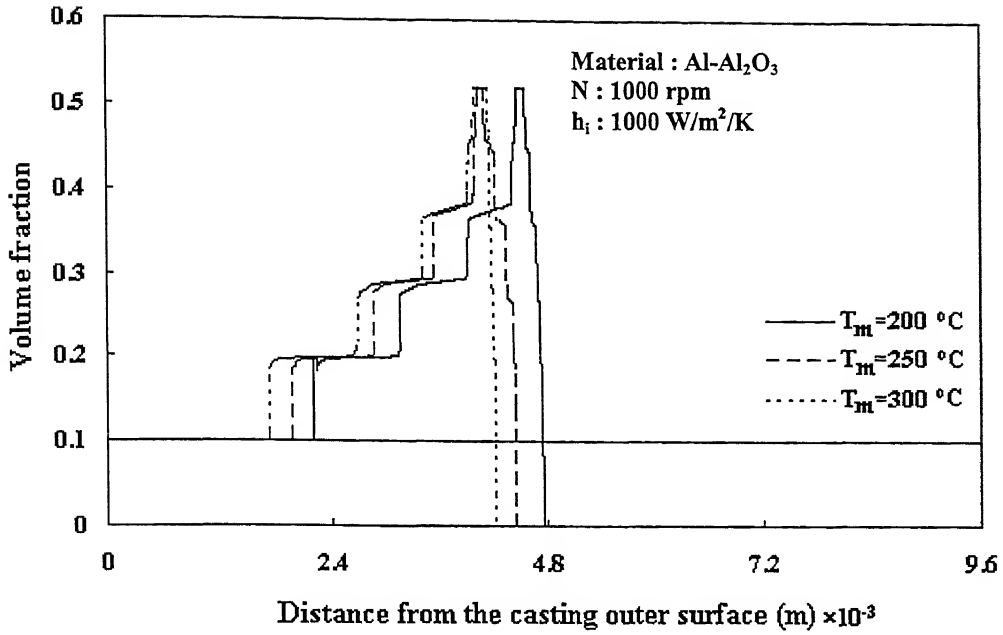

Figure 4.10: Effect of mold temperature on the particle segregation pattern for 1μm particle size

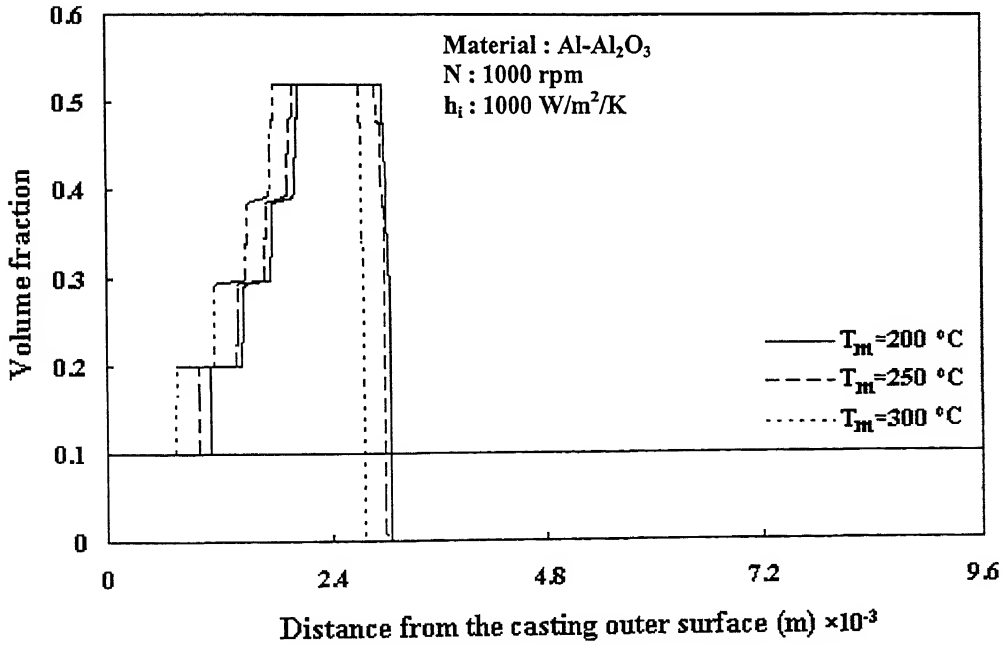

Figure 4.11: Effect of mold temperature on the particle segregation pattern for 2μm particle size

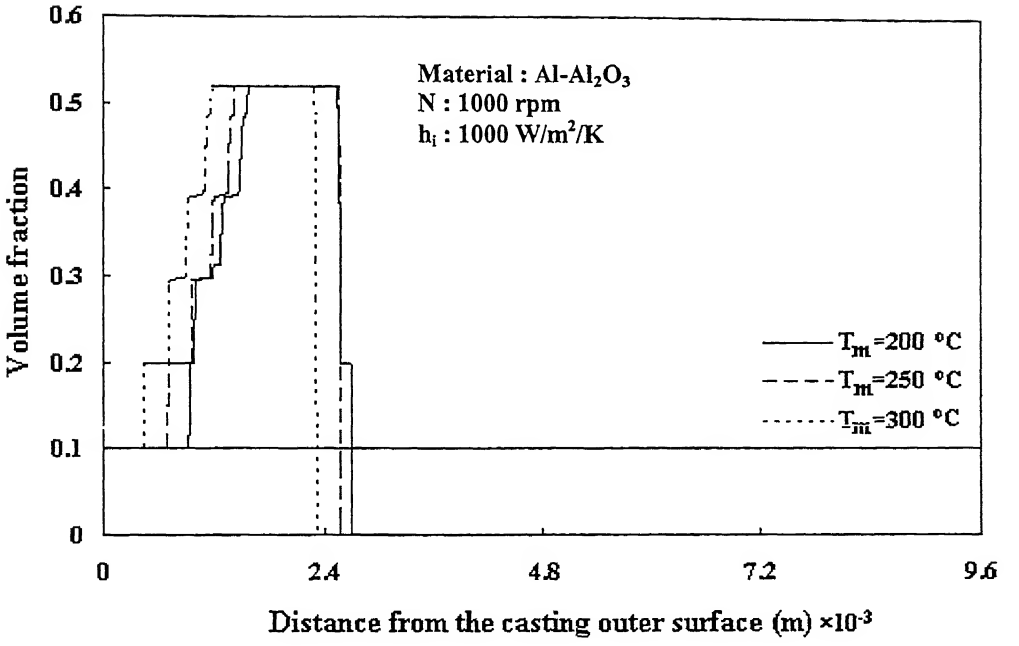

Figure 4.12: Effect of mold temperature on the particle segregation pattern for 3μm particle size

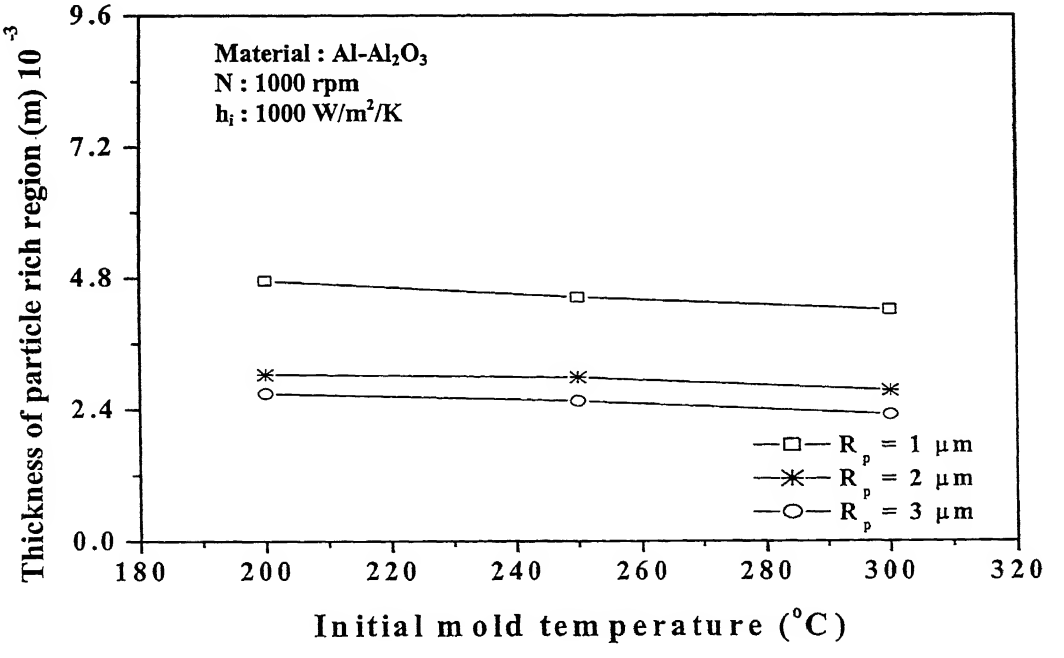

4.13: Influence of initial mold temperature (T_M) on the variation of thickness of particle rich region of $Al\text{-}Al_2O_3$ composite

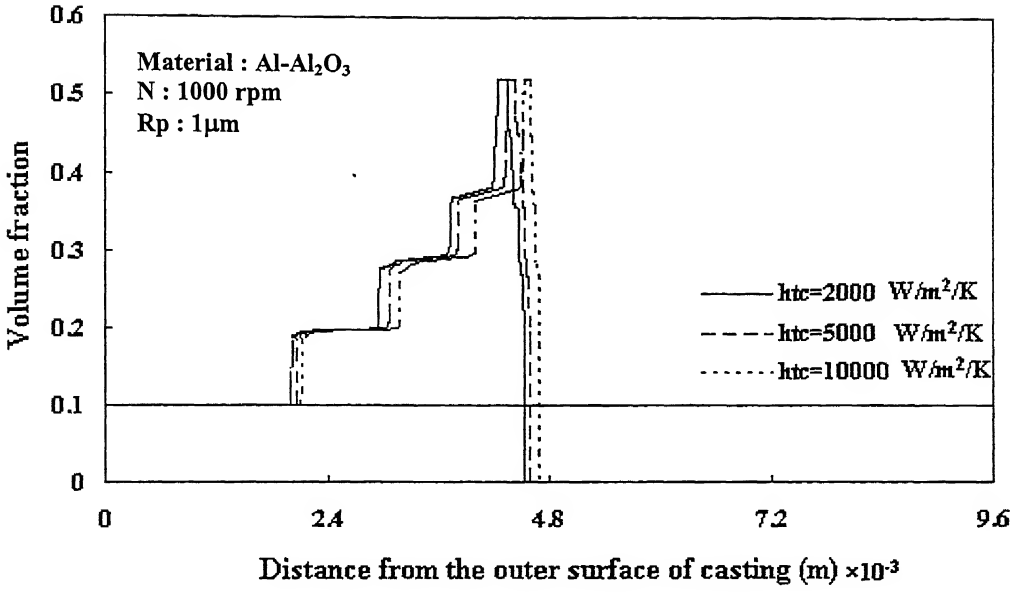

Figure 4.14: Effect of heat transfer coefficient on the particle segregation pattern for 1 μm particle size

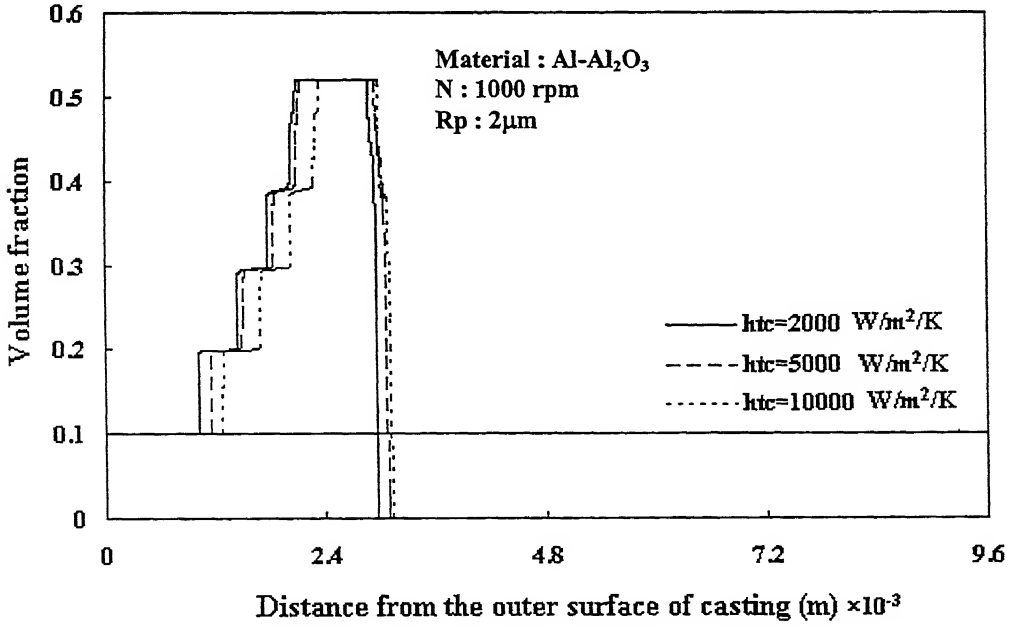

Figure 4.15: Effect of heat transfer coefficient on the particle segregation pattern for 2 μm particle size

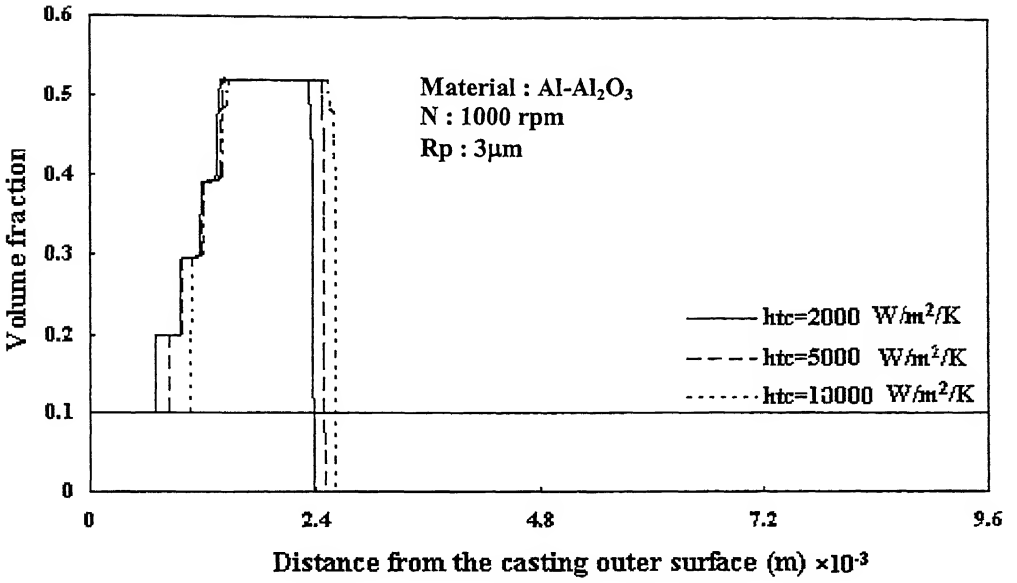

Figure 4.16: Effect of heat transfer coefficient on the particle segregation pattern for 3 μm particle size

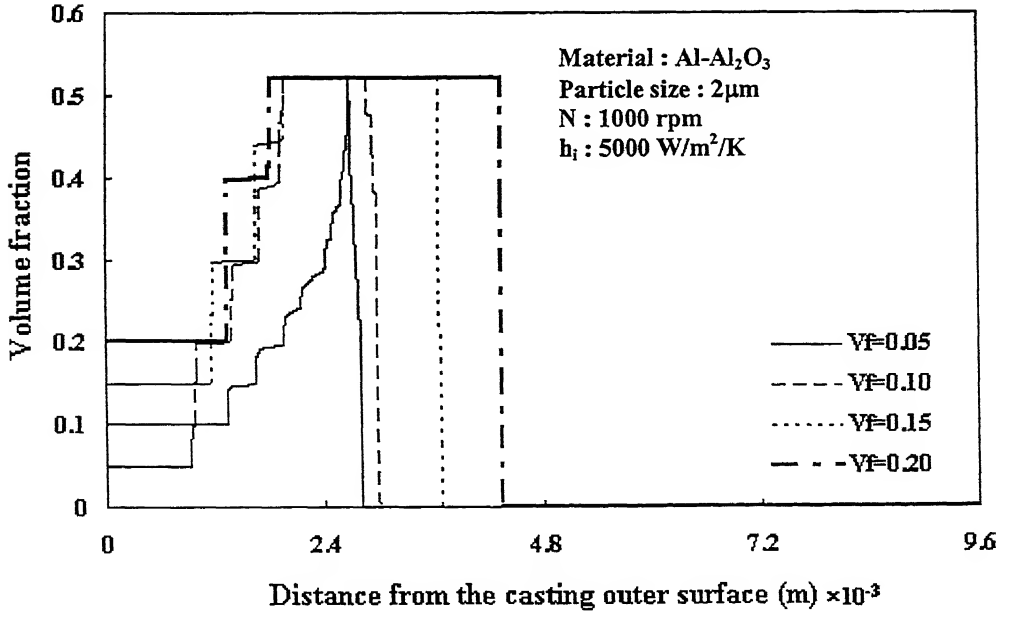

Figure 4.17: Effect of initial volume fraction of particulates on particle segregation pattern

rich regions increases with increase in the initial volume fraction of the particulates. This is because, the increase in the initial volume fraction of the particles in the melt increases its viscosity, thereby reducing the motion of the particles which results in larger particle rich region due to reduced segregation.

4.1.8 Effect of Solidification Time:

Figures 4.18 to 4.23 show the variation of volume fraction of the particulates with time for three different particle sizes, namely, 1, 2 and 3μm. The heat transfer coefficient at the metal/mold interface is taken as 2000 $W/m^2/K$ in Figs. 4.18 to 4.20 and 5000 $W/m^2/K$ for Figs. 4.21 to 4.23. All other parameters are kept fixed. From these figures it is evident that with increase in solidification time particles get more time to move in the liquid melt leading to more intense particle segregation. It is also observed that with increase in particle size or decrease in heat transfer coefficient, there is a reduction in particle rich region - this has already been discussed earlier in sections 4.1.2 and 4.1.6. It is noted that, the heat transfer coefficient and particle size are two important controlling parameters in deciding the particle segregation pattern. With increase in heat transfer coefficient, the heat removal rate increases leading to decrease in solidification time resulting in the increase in particle rich region. The final thickness of the particle rich region for $Al\text{-}Al_2O_3$ varies from 4.524×10^{-3} to 2.44×10^{-3} m and 4.702×10^{-3} to 2.55×10^{-3} m for the values of heat transfer coefficient 2000 and 5000 $W/m^2/K$ respectively, as the particle size increases from 1 to 3 μm.

As solidification proceeds, thickness of the air-gap formed at the metal/mold interface increases due to the contraction of the casting as well as thermal expansion of the mold. This results in the reduction of the heat transfer coefficient at the interface with time. Thus the rate of solidification decreases as the solidification front progresses from the outer periphery of the casting towards its center - this is evident in Figs. 4.18 to 4.23.

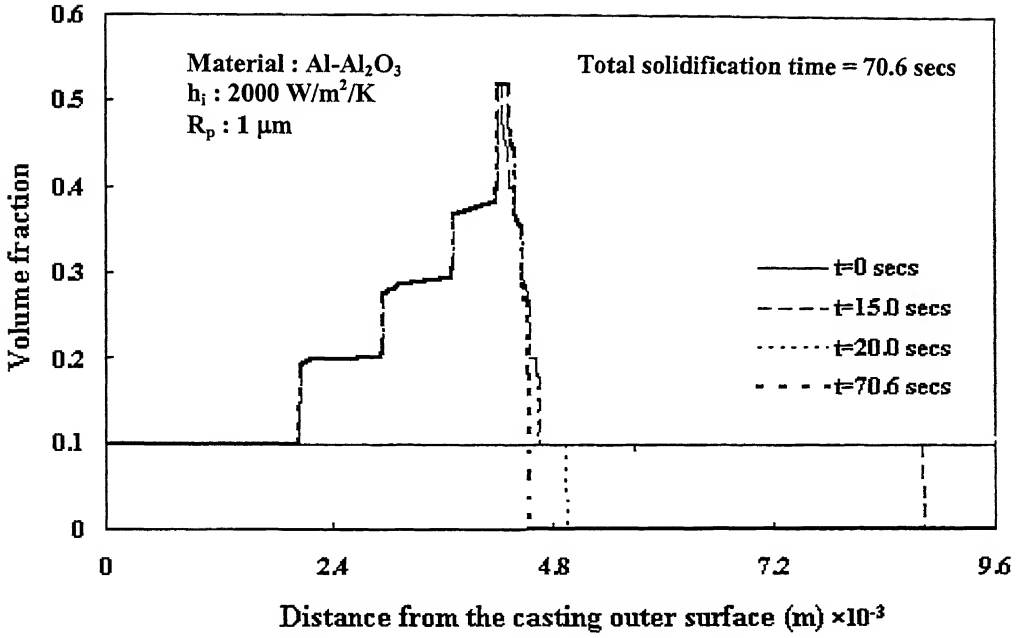

Figure 4.18: Variation of volume fraction with time for 1 *μm* particle size

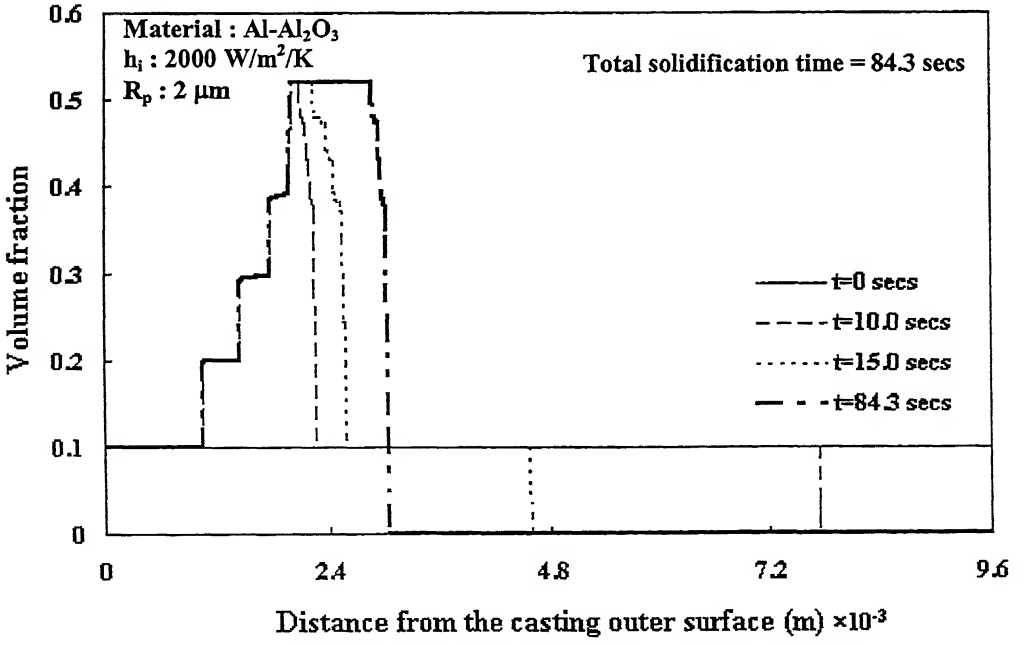

Figure 4.19: Variation of volume fraction with time for 2 *μm* particle size

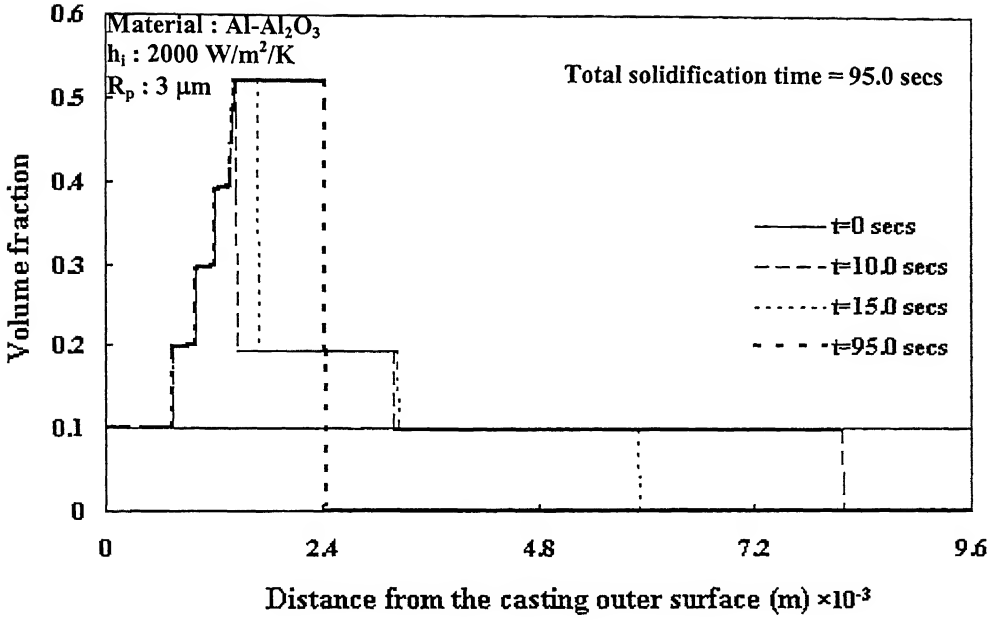

Figure 4.20: Variation of volume fraction with time for 3 *μm* particle size

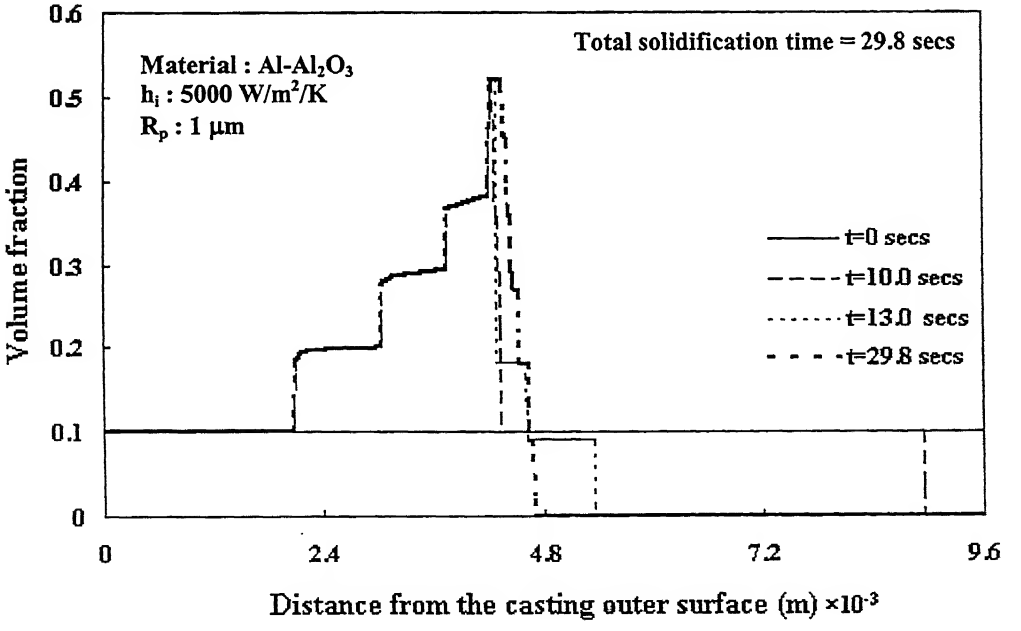

Figure 4.21: Variation of volume fraction with time for 1 *μm* particle size

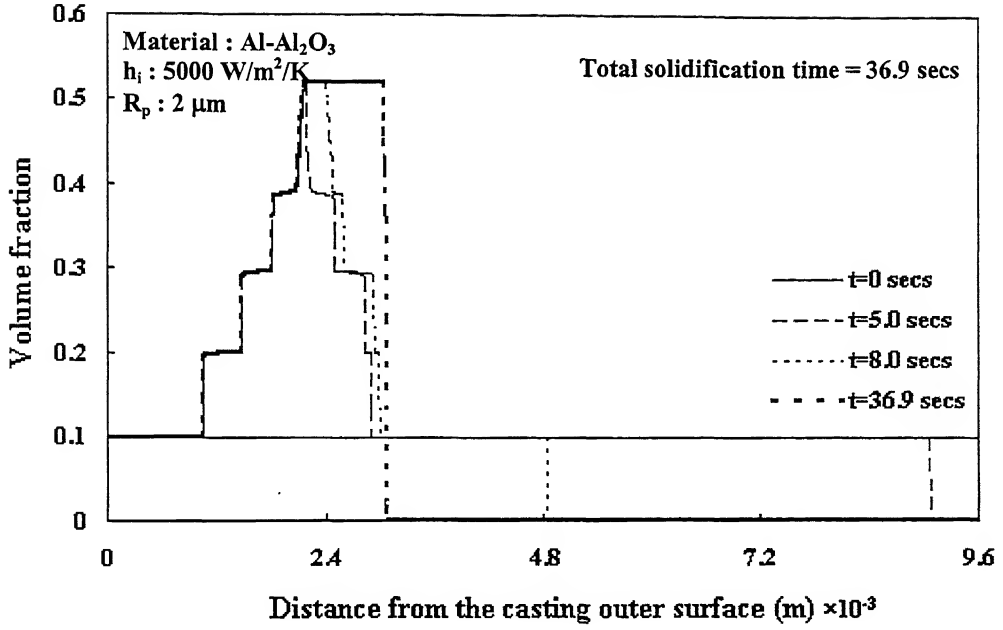

Figure 4.22: Variation of volume fraction with time for 2 μm particle size

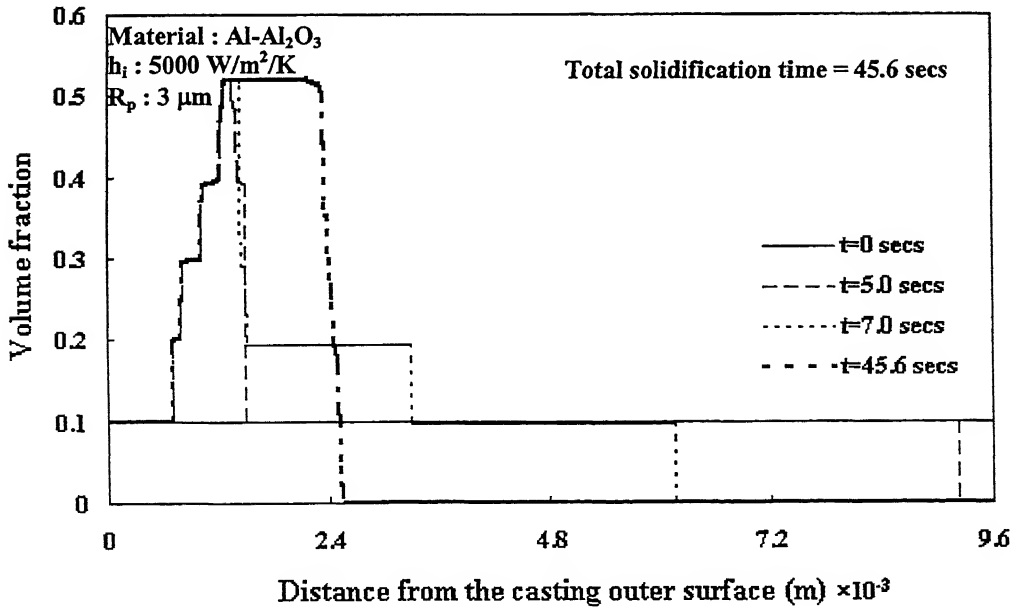

Figure 4.23: Variation of volume fraction with time for 3 μm particle size

4.2 CALCULATION OF SOLIDIFICATION TIME:

For various sets of operating conditions, the time required for complete solidification of the casting has been calculated. The results of these simulations are presented in the form of total solidification time.

4.2.1 Effect of Initial Pouring Temperature:

Figure 4.24 shows the effect of initial pouring temperature on the complete solidification time for three different particle sizes, namely, $1\mu m$, $2\mu m$ and $3\mu m$. The initial pouring temperatures taken in the simulations are 650, 730 and 800 ^{o}C. All other parameters are kept the same. It is observed that the total solidification time increases with increase in the initial pouring temperature. This is due to the fact that with increase in the initial pouring temperature the total heat content in the melt increases and thus more time is required to withdraw this extra heat. It is also seen that the total solidification time increases with increasing particle size. It has already been discussed in the earlier section that particle segregation becomes more intense with increase in the particle size. Since Al_2O_3 particles are heat-resistant, increase in the volume fraction of these particles near the outer periphery of the casting decreases the thermal diffusivity in that region substantially. This results in decrease in heat removal rate, which, in turn, leads to increase in the solidification time.

4.2.2 Effect of Initial Mold Temperature:

Figure 4.25 is a plot between the initial mold temperature and solidification time for three different particle sizes, namely, $1\mu m$, $2\mu m$ and $3\mu m$. The initial mold temperatures used in these simulations are 200, 250 and 300 ^{o}C. All other parameters remain the same. From the figure it is evident that the time required for complete solidification of the casting increases with increase in the initial mold temperature for all the three particle sizes. As the initial mold temperature increases, the temperature gradient between the casting and the mold decreases reducing the heat transfer rate. This

4.2.3 Effect of heat transfer coefficient at the metal/mold interface:

Figure 4.26 shows the effect of heat transfer coefficient at the metal/mold interface on the complete solidification time for three different particle sizes. The h_i values used here are 1000, 2000 and 5000 $W/m^2/K$. All other parameters are the same. It is observed that with increase in the heat transfer coefficient the complete solidification time decreases as the rate of heat removal becomes faster.

4.2.4 Effect of Particulate Volume Fraction:

Figure 4.27 shows the variation of total solidification time as a function of initial particulate volume fraction. As the initial volume fraction of the particulate increases, the effective thermal diffusivity of the composite decreases resulting in longer solidification time.

4.3 TEMPERATURE DISTRIBUTION IN THE CASTING AND MOLD REGIONS:

The temperature profiles in the casting as well as mold regions have been calculated by solving the governing differential equations with appropriate boundary conditions along with the energy balance equation discretized in *Finite Volume Technique*, which is described in the chapter 3. Figure 4.28 shows the variation of temperature as a function of time for both the casting and mold regions. It is seen that in the final temperature distribution, there is a temperature drop at the casting/graphite as well as at the graphite/steel mold interfaces.

Figure 4.29 shows the effect of variation of heat transfer coefficient on temperature distribution in both the casting and mold regions. Here, the heat transfer coefficients used are 1000, 2000 and 5000 $W/m^2/K$. All other parameters are fixed as earlier. It is observed that the temperatures at the inner and outer surfaces of the graphite mold increase with the increase in the heat transfer coefficient. This attributes to the fact that the higher heat transfer coefficient signifies better thermal contact between the

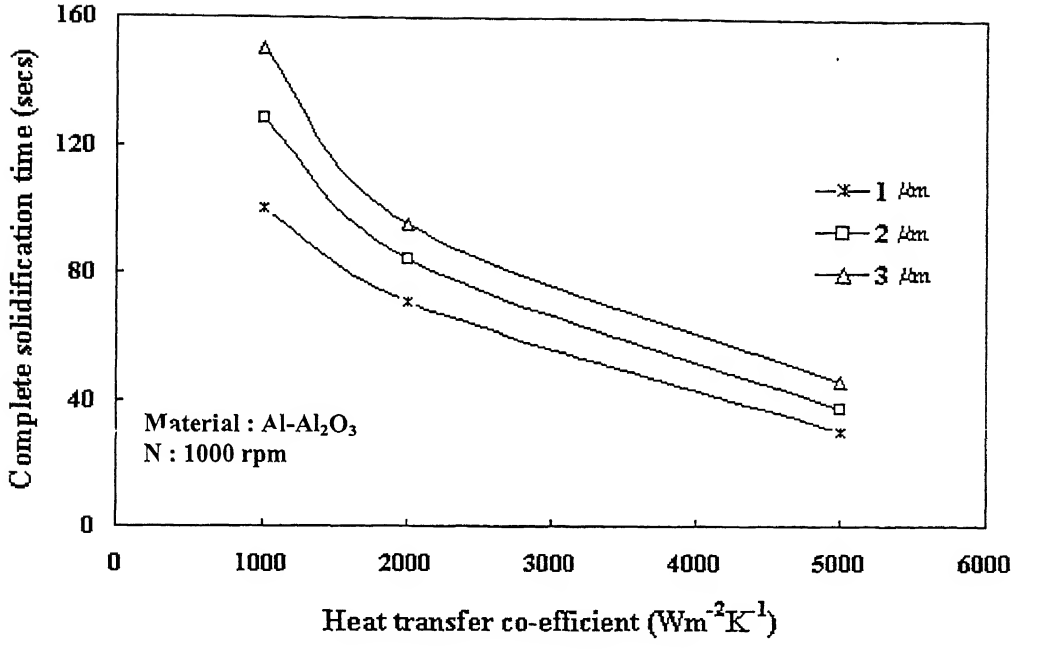

Figure 4.26: Effect of heat transfer co-efficient on solidification time for different particle size

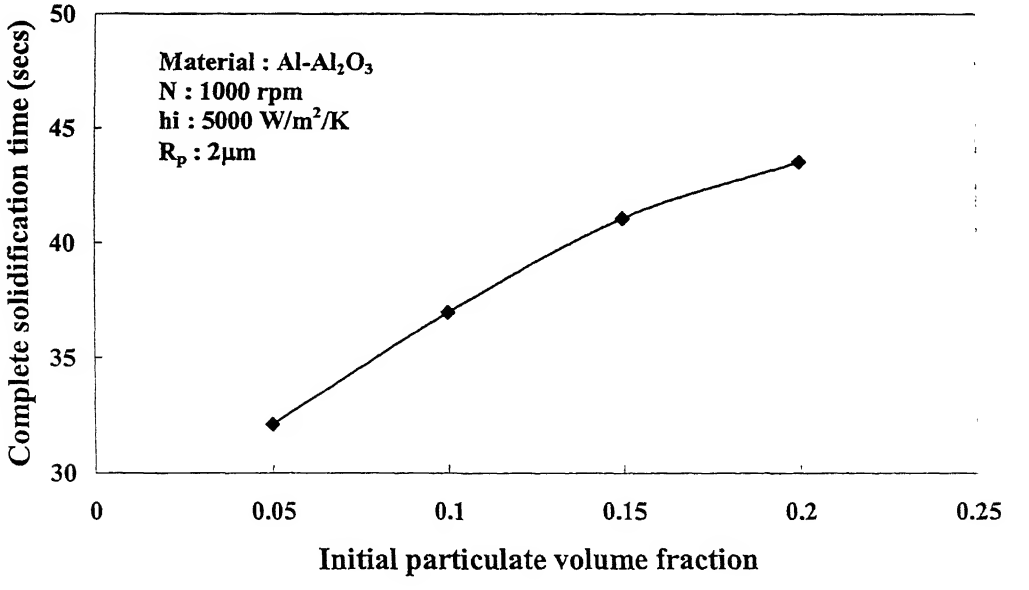

Figure 4.27: Effect of initial particulate volume fraction on solidification time

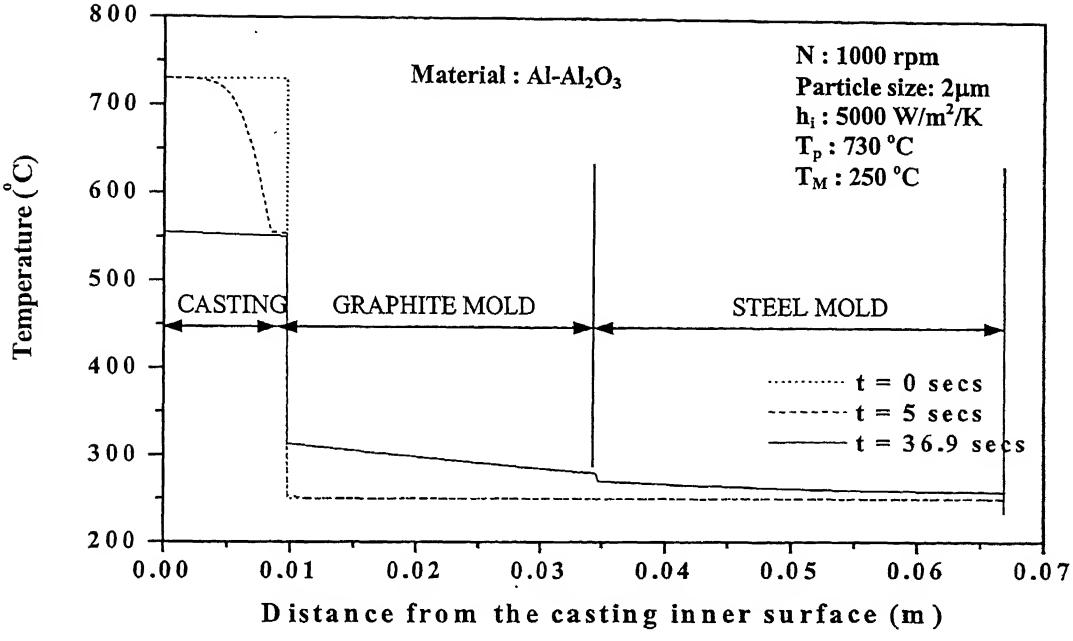

Figure 4.28: Variation of temperature as a function of time for both the casting and mold regions

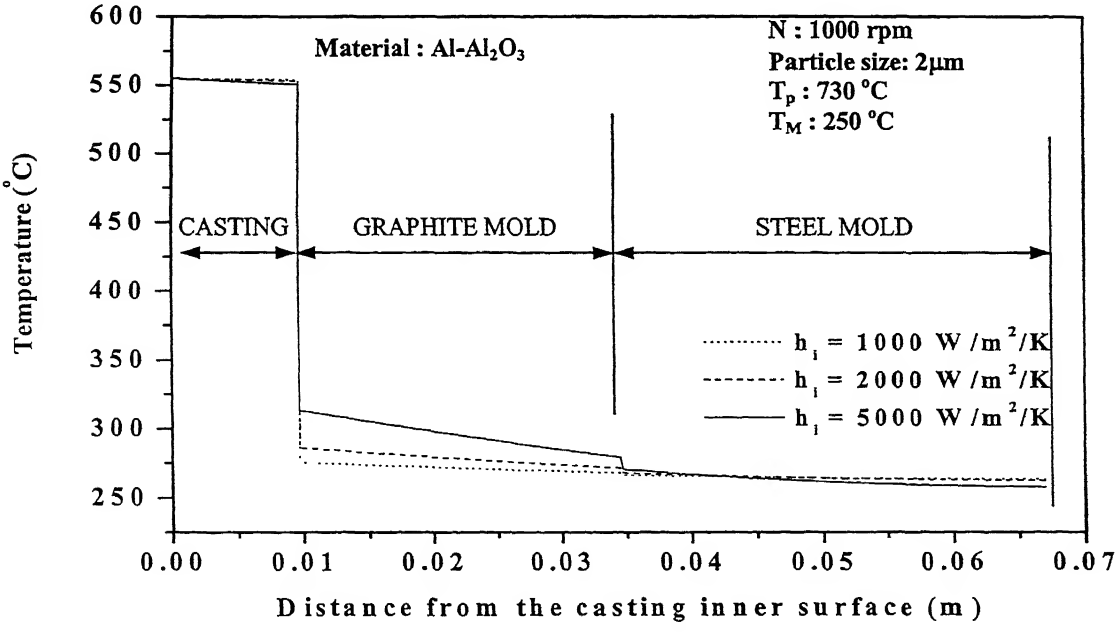

Figure 4.29: Effect of heat transfer co-efficient on the temperature distribution for both the casting and mold regions

casting and the mold wall resulting in more intense heat transfer from the casting to the mold. On the other hand, the reduction in the heat transfer coefficient at the interface results in lesser heat transfer and therefore lower temperature at the interfaces.

4.4 DISCUSSIONS:

Siva Raju and Mehrotra [9] have presented a mathematical formulation based on one-dimensional heat transfer analysis incorporating variation in thermo-physical properties due to particle movement in the matrix. The present investigation is an attempt to further improve that analysis. Both Kang and Rohatgi [7] and Siva Raju and Mehrotra [9] in their models neglected the repulsive force term in their equations for force balance on particles. In the present investigations, the repulsive force, which a particle experiences when it approaches a solid wall/solidification front is taken into consideration and characterized by an appropriate expression. Again, in the work of Siva Raju and Mehrotra, variation of volume fraction of particles with time is considered by ensuring conservation of total mass of particles at all times. In their work, the volume of particulates in between two consecutive nodal points always remains same. So, in that case the length of the segment varies with time and so are the nodes as they depend on constant volume fraction of particulates. But in the present formulation the nodes are fixed for all time and the variation of volume fraction of particles in any particular segment with time is calculated by taking into account the particle movement with time. One of the important features of the present model is the use of *finite volume technique* as the solution procedure unlike the finite difference scheme used in the previous work [10]. The advantage of finite volume method over finite difference one is the automatic conservation of all physical quantities unlike the approximation of so in the later case.

It is observed in sections 4.1.1 to 4.2.4 that the particle segregation depends on the rotational speed of the mold, size of the reinforcing material, relative density difference between the matrix and reinforcement material, initial pouring temperature of the liquid melt, pre-heating temperature of the mold, heat transfer coefficient at the casting/mold interface and the initial volume fraction of the particulates in the melt. The solidification

time gets influenced mainly by the heat transfer co-efficient at the casting/mold interface and initial temperatures of the liquid melt and mold.

Formulation of the model is based on assumptions, several of which are only partially valid. For instance, the assumption of interface between the solid and liquid region to be planar is only approximate. Strictly speaking, the solidification front can be planar, cellular or dendritic depending upon the rate of solidification. It is very difficult to predict either cellular or dendritic morphology of the solidification front, hence the assumption of planar solidification front is made.

The assumption of negligible thermal resistance between the particles and melt can also be questioned. In actual practice, there may be some solubility of solid particulates in the liquid matrix, or some chemical reaction between the two. In both cases, there may be a heat of reaction associated with the phenomena taking place at the surface of the particles. This heat may appear as the heat source at the particle/melt interface. Further, a chemical reaction at the surface may result in the formation of a product layer which offers thermal resistance to the heat flow, resulting in distortion of the temperature field around the particle. This may, in any case, happen also due to the difference in thermal conductivities between the particle and the melt.

The assumption of temperature invariant thermal properties is just for convenience only. If reliable expressions for thermal properties as a function of temperature are available, these can be easily incorporated in the model equations.

Dependence of heat transfer coefficient at the casting/mold interface on the rotational speed is assumed to be negligible here. But it has been established that for aluminium, the heat transfer coefficient at the metal/mold interface increases with increase in the rotational speed [34]. The reason is that at a higher rotational speed, liquid metal puts a larger pressure on the solidified layer which, in turn, results in a better physical contact between the solidified layer and mold wall, improving the heat transfer coefficient at this interface. So, the effective heat transfer coefficient at the metal/mold interface can be found out using a suitable relation and this relation along with Eq. (2.14) will give a better estimate of variation of the effective heat transfer coefficient with time.

For simplicity, initial position of the particles are considered at the nodal points. But it is assumed that particles are uniformly distributed in the melt. Uniformity of

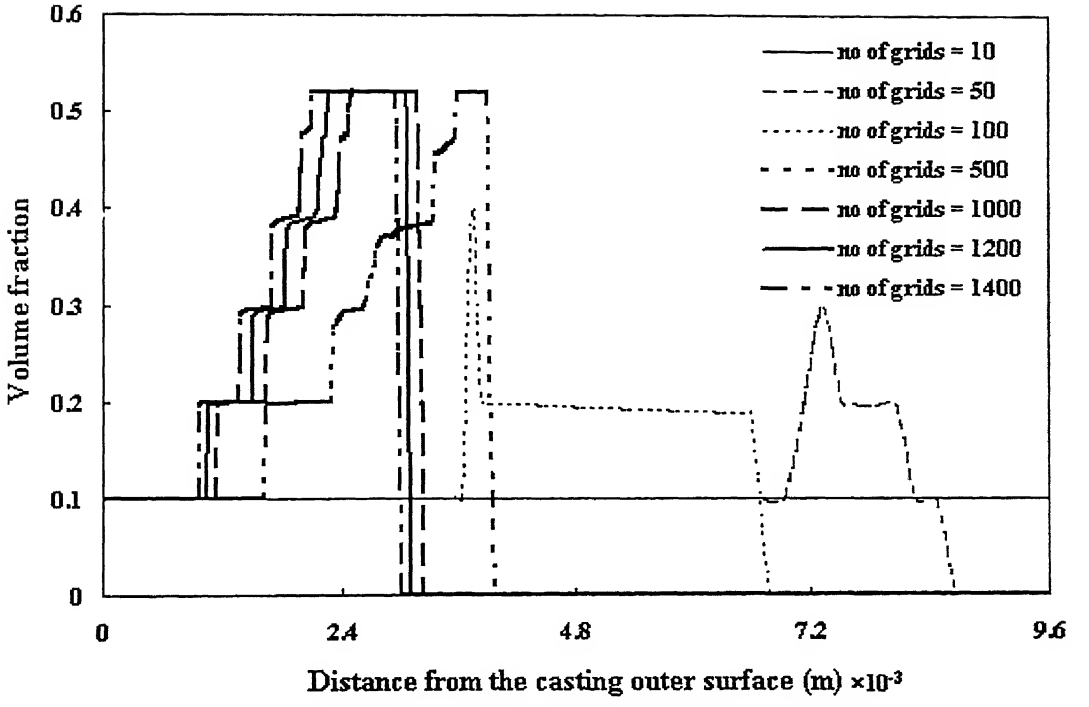

Figure 4.30: Particle segregation pattern w.r.t. the number of grids

particulate distribution can be described more effectively with larger nodal points. Higher number of nodes imply lesser grid size. But there is a limit beyond which the grid size can not be lowered since it has to be greater than the particle diameter. Figure 4.30 shows the variation of particle segregation pattern in the solidified melt with number of grids for $Al\text{-}Al_2O_3$ system. It is observed in the figure that, with higher number of nodes, clustering of the particles is seen closer towards the outer surface of the casting and for 1000, 1200 and 1400 number of grids, the segregation pattern assumes a similar shape and almost near to one another. But it is noted that, when the number of grids are 10, the volume fraction of particles in the solidified composite becomes equal to that of the initial melt. This is because, with a highly reduced number of grids, the distance between the particles increases. As a result of which particles have to travel farther distances to enter into the adjacent volume segment, which require a longer time. Here it can be inferred that, particles do not get proper time to move to the adjacent volume segment to form cluster and get trapped by the solidification front when they are in the same segment as those of the initial ones.

While trying to converge the time step in the program, several improvements have to be incorporated to achieve a much reduced convergence criteria (10^{-8}), to be ensured of the fact that the numerical technique is close to the exact solution. The improvements made were as follows.

- To calculate the values of ρ, c and k for any interface of the control volume, harmonic mean of the adjacent nodal point values have been taken instead of arithmetic mean.
- Throughout the program, all the calculations have been carried out with double precision to minimize the round-off error.
- Value of π used here is 22/7 instead of 3.14.

CHAPTER 5

SUMMARY AND CONCLUDING REMARKS:

The present investigation is carried out with the objective of improving upon the already formulated mathematical model to describe the centrifugal casting of metal matrix composites. The model aims to describe the temperature distributions throughout the casting and the mold regions and particle segregation pattern in the casting region. In the present investigation *Finite Volume Technique* has been employed in place of earlier used finite difference based solution scheme. In the force balance expression, one significant improvement in the model formulation is repulsive force term is incorporated for the particles that are at the vicinity of the solid/liquid interface. This modified expression is used to calculate the particle segregation pattern in the casting region. The influence of different process parameters such as rotational speed of the mold, particle size, relative density difference between the particle and the melt, initial mold temperature, pouring temperature, heat transfer coefficient at the casting/mold interface on the solidification time of the casting and on the segregation pattern of the particles is studied.

The main conclusions of this investigations can be summarized as follows:

- Thickness of the particle rich region in the composite decreases with increase in rotational speed, particle size, relative density difference between the particle and the melt, initial pouring temperature and initial mold temperature.
- With decrease in the heat transfer coefficient at the casting/mold interface, the rate of heat transfer decreases leading to increase in the solidification time which, in turn, results in more intense segregation of solid particulates.
- With increase in the initial volume fraction of solid particulates, both the solidification time as well as the final thickness of the particulate rich region increase.
- Rate of solidification is very fast at the beginning, which is more than that of the particle velocity due to centrifugal force. Due to this, the particles adjacent to the

casting/mold interface do not get a chance to move towards the casting/mold interface in the cases of *Al-Al_2O_3* and *Al-SiC* systems to form a cluster. As a result of which, the volume fraction of the particulates in the solidified composite is the same as that of the initial volume fraction in the melt which can be visualized by the horizontal portions of the figures in the cases of *Al-Al_2O_3* and *Al-SiC* systems. So, in case of *Al-Al_2O_3* and *Al-SiC,* the maximum clustering of particles is seen after a certain distance from the casting/mold interface. But in case of *Al-Gr* system, particles move towards the inner periphery and form maximum segregation there. It is also seen that for 1 μm particle size in case of *Al-Gr* system, the volume fraction of the particles in the solidified composite, in the volume segment, just adjacent to that of the casting/mold interface remains same as that of the initial volume fraction in the melt unlike to that of 2 and 3 μm particle size.

REFERENCES:

[1]. B.D.Agarwal and L.J.Broutman , "*Analysis and performance of Fiber Composites*", 2nd edition, John Wiley & Sons Inc. pp. 1- 2.

[2]. P.Rohatgi, "*Cast Metal Matrix Composites: Past, Present and Future*", AFS Trans.(2001), vol.109, pp. 633-657.

[3]. S.Suresh, A.Mortensen and A. Needleman, " *Fundamentals of Metal Matrix Composites*", Butterworth-Heinemann, London, (1993), p.3, p. 319.

[4]. D.Nath and P.K.Rohatgi, "*Segregation of Mica Particles in Centrifugal and Static Castings of Al-Mica Composites*", Composites, (1981) pp.124-128.

[5]. B.P.Krishnan, H.R.Shetty and P.K.Rohatgi, "*Centrifugally Cast Graphitic Aluminium with segregated Graphite Particles*", AFS Trans.,(1976), vol.76, pp.73-80.

[6]. L.Lajoye and M.Suery, "*Centrifugal Casting of Aluminium alloy matrix composites*", Solidification Processing 87, Sheffield 21-24 sept., (1987), pp.443-446.

[7] C.G.Kang and P.K.Rohatgi, "*Transient thermal analysis of solidification in a centrifugal casting for composite materials containing particle segregation*", Metall.Trans.B. (1996), vol.27B, pp. 277-285.

[8] L. Lajoye and M.Suery, "*Modelling of particle segregation during centrifugal casting of Al-Matrix composites*", Publ. ASM Intl., (1988), pp. 15-20.

[9] P.Samba Siva Raju and S.P.Mehrotra, "*Mathematical Modelling of centrifugal casting of metal matrix composites*", Materials Transactions, JIM, Vol.41, No.12 (2000) pp.1626-1635.

[10] P. Samba Siva Raju , "*Mathematical modeling of centrifugal casting of Metal Matrix Composites*" , M.Tech. Thesis, Dept. Materials and Metallurgical Engineering, I.I.T., Kanpur India, May, (1999).

[11]. D.M.Stefanescu, A. Moitra, A.S. Kacar, and B.K. Dhindaw, " *The Influence of Buoyant Forces and Volume Fraction of Particles on The Particle Pushing/ Entrapment*

Transition During Directional Solidification of Al-Sic And Al-Graphite Composites", Metall. Trans. A. (1990), vol. 21A, pp. 231-239.

[12]. R.Sasikumar and B.C.Pai, "*Redistribution of Second-Phase Particles in Melt during Solidification: Computer Model*", Solidification Processing 87., Sheffield 21-24 sept., (1987), pp. 443-446.

[13]. P.K.Mallick, "*Composites Engineering Handbook*", Marcel Dekkar Inc., USA, (1997), pp. 638-640.

[14]. J.Szekely, " *Fluid Flow Phenomena in Metal Precessing*", Academic Press, New York, NY, (1979), pp. 255-263.

[15]. R.Sasikumar and T.R. Ramamohan, (1991), " *Distortion of the temperature and solute concentration fields due to the presence of particles at the solidification front- effects on particle pushing*", Acta metal. Vol (39), No. 4, pp. 517-522.

[16]. G.F. Bolling and J. Cisse, (1971), " *A Theory for the Interaction of Particles with a Solidifying front*", J. Cyrst. Growth, vol (10), pp.56-66.

[17]. R.R.Gilpin, (1980), " *Theoretical studies of Particle Engulfment*", J. Coll. Interface Sci, vol (74), pp. 44-63.

[18]. A.A. Chernov, D. B. Temkin and A. M. Melnikova, (1976), " *Theory of the capture of Solid Inclusions during the Growth of crystals from the melt*", Soviet. Phys. Cyastallogr., vol (21), pp. 369-374.

[19]. R.Sasikumar and M. Kumar, 1991, " *Redistribution of Particles During Casting of Composite Melts: Effects of Buoyancy and Particle Pushing*", Acta metal. Mater. Vol 39, No. 11, pp. 2503-2508.

[20]. Sannomiya, N., Matuda, K., 1987. "*Least squares parameter estimation in fish behavior model*", Bull.jpn. Soc. Sci Fish. 53 (11), 1951-1957.

[21]. Takagi, T., Nashimoto, K., Hiraishi, T., 1993. "*Fish schooling behavior in water tanks of different shapes and sizes*", Bull.jpn. Soc. Sci Fish. 59 (8), 1279-1287.

[22]. Roschen Sasikumar, 1992, " *Discussion of "Behavior of Ceramic Particles at the Solid-Liquid interface in Metal Matrix Composites*", Metallurgical Transactions A, Vol (23A), pp. 2326-2330.

[23]. M.N.Ozisik, "*Finite Difference Methods in Heat Transfer*", CRC Press, London, (1994), pp. 134-138 and 281-296.

[24]. S.V.Patankar, " *Numerical Heat Transfer and Fluid Flow*", Hemisphere, (1980), pp. 25-74.

[25]. F.Mampaey, " *Examination of Finite Volume method for Simulating Casting Process*", AFS Trans.(2000), vol. 108, pp. 531-540.

[26]. R. B. Bird, W. E. Stewart and E. N. Lightfoot, "*Transport Phenomena*", John Wiley & Sons, New York (1960), pp. 354-357.

[27]. H. S. Carslaw and J. C. Jaeger, "*Conduction of Heat in Solids*", Oxford University Press (1959) , p.101, p.200.

[28]. Andrew Gray, G.B.Mathews, "*A Treatise on Bessel Functions and their Applications to Physics*", 2nd edition (1922), p – 300.

[29]. E.T.Goodwin, J.Staton , " *Table of $J_0(j_{0,n}\, r)$* ", Quart.J.Mech.Appl.Math.I (1948), pp. 220-224.

[30]. R.S.Gupta and Dhirendra Kumar, "*Variable Time Step methods for One-Dimensional Stefan Problem with Mixed Boundary Condition*", Int. J. Heat and Mass Transfer (1981), vol. 24, pp.251-259.

[31]. ASM Speciality Handbook, "*Aluminium and Aluminium alloys*", ASM International, (1994), p. 718.

[32]. Metals Handbook, 10th ed., ASM International, Materials Park, OH, (1992), vol. 2, p. 164.

[33]. Y. Nishida, W. Droste and S. Engler, " *The Air-Gap Formation Process at the Casting-Mold Interface and the Heat Transfer Mechanism through the Gap*", Mett. Trans., B (1986) vol. 17, pp. 833-844.

[34]. M.R.R.I.Shamsi, " *Formulation and Validation of a Two-Dimensional Heat and Fluid Flow Model of Single Roll Continuous Sheet Casting Process*" Ph.D. Thesis, Dept. Materials and Metallurgical Engineering, I.I.T., Kanpur India, (1994).